

Reactive Packed Bed Safety: Experimental Evaluation of TiCl_4 Passivation for Metal Hydrides

A Major Qualifying Project Submitted to the Faculty of
WORCESTER POLYTECHNIC INSTITUTE
In partial fulfillment of the requirements of the
Degree of Bachelor of Science

Authors

Alexander Grealley

Gavin Maloney

Jonathan Santos

Adrianna Tagayun

April 24th, 2024

Report Submitted to:

Professor Andrew Teixeira

Professor Stephen Kmietek

Worcester Polytechnic Institute

This report represents the work of WPI undergraduate students submitted to the faculty as evidence of completion of a degree requirement. WPI routinely publishes these reports on its website without editorial or peer review. For more information about the projects program at WPI, please see <http://www.wpi.edu/academics/ugradstudies/project-learning.html>

Acknowledgements

We extend our sincere gratitude to Honeywell for providing both the opportunity and funding that propelled the advancement of safety measures in next-generation fuel cells. A special appreciation goes to Dr. Matt Kale for his invaluable expertise and insightful contributions to the project. We would like to thank Professor Andrew Teixeira and Professor Stephen Kmietek for their guidance and support throughout the entire project process. We would also like to thank Januario Da Costa and David Kenney, PhD students in WPI's Chemical Engineering (CHE) department, for their crucial assistance with the group's experiments. Furthermore, our group is thankful to Dr. Geoffrey Tompsett (CHE – assistant research Professor), Douglas White (CHE – electronics engineer), Doug Leonardi (Physics Department – Operations Manager) for assisting us in characterization experimentation as well as Ian Anderson (CHE – Lab Manager & Advanced Machinist) for helping set up our TiCl_4 experimentation apparatus. Lastly, we acknowledge Worcester Polytechnic Institute for generously providing laboratory resources that were instrumental in conducting our MQP project.

Abstract

The goal of this study is to evaluate volatile liquid TiCl_4 as a passivation method for hydrogen generation using metal hydrides. A hydrogen fuel cell is advantageous in its efficiency, long-term storage, zero emissions, and quiet process in engines. However, operation and transport processes encompass safety concerns as the fuel cell's primary reaction— LiAlH_4 hydrolysis—may undergo undesired thermolysis due to high reactivity. Ex-situ characterization of (spent and unspent) fuel properties was performed along with batch and flow experiments to determine the effectiveness of TiCl_4 passivation. SEM-EDX imaging revealed titanium and chlorine deposited onto the surface of TiCl_4 treated spent fuel, particularly when subjected to the PBR process. DRIFTS characterization revealed potential reactivity hazards, as evidenced by the retention of half of the water content in the samples even at temperatures exceeding 250°C . Further testing is needed for improving coating extent as well as determining its effectiveness as a passivation layer around spent fuel and LiAlH_4 metal hydride.

Table of Contents

Acknowledgements	1
Abstract	2
Table of Contents	3
List of Tables	4
List of Figures	5
1. Introduction	6
1.1 Project Objectives	6
2. Background	7
2.1 PEM Fuel Cell	7
2.2 Metal Hydrides for Hydrogen Storage	7
2.2.1 Hydrogen Desorption Improvements with Titanium	8
2.3 Lithium Aluminum Hydride	8
2.3.1 Handling LAH	9
2.4 Surface Passivation	10
2.5 Spent Fuel Composition	11
2.6 Characterization Methods	11
2.6.1 DRIFTS	11
2.6.2 SEM-EDX	12
2.6.3 XRF	12
2.6.4 Raman Spectroscopy	13
3. Methods	14
3.1 Materials	14
3.2 Synthesis of Titanium Coating Experimentation	14
3.2.1 Reagent Preparation	14
3.2.2 System Preparation	14
3.2.3 Batch Reactor Experiment	15
3.2.4 Packed Bed Reactor Experiment	16
3.3 Preparing for Characterization	17
4. Results and Discussion	18
4.1 Batch and Flow TiCl_4 Coating Experiments	18

4.2 Spent Fuel Characterization.....	19
4.2.1 SEM-EDX	19
4.2.2 X-Ray Fluorescence Spectroscopy	21
4.3.3 Raman Spectroscopy	23
4.3.4 DRIFTS	25
5. Conclusion & Recommendation.....	27
6. References	29
Appendix A – Spent Fuel Characterization	32
A.1 Optical Microscopy	32
A.2 SEM Scans	35
A.3 SEM-EDX Spectra.....	39
A.4 XRD Spectra	40
A.5 TGA Analysis	42
Decomposition Kinetics.....	42
Adsorption Thermodynamics.....	43
Appendix B – Preliminary Batch Experimentation.....	46
Appendix C - Flow Experiment Calculations.....	48
C.1 Saturated Vapor Density Calculations.....	48
C.2 Theoretical Yield Calculations	50
C.3 Water Sorption Testing	50
C.4 Mass Flow Controller Calibration Curves	51

List of Tables

1. Short List of Lithium Aluminum Hydride Properties.....	8
2. List of Chemical Compounds Used.....	14
3. List of Potential Raman Peak Identifications	24
4. List of TGA Runs.....	44
5. Antoine Equation Constants & Calculated Values at 298 K	49
6. Saturated Vapor Density of TiCl ₄ and H ₂ O at 298 K.....	50
7. Experimental Parameters of Flow Synthesis Experiment	51
8. Experimental Runs of Water Sorption Testing.....	51

List of Figures

1. Illustration of a PEM Cell	7
2. Flow Diagram of Batch Reactor System	15
3. Flow Diagram of Plug Flow Reactor System	16
4. SEM-EDX Images of Spent Fuel Samples after TiO ₂ Coating	20
5. Surface Metal Weight Percents in XRF	22
6. Normalized Raman Spectroscopy Data	23
7. DRIFTS Spectra of Spent Fuel and Hydrated Batch Sample	26
8. Optical Microscope Images of Al ₂ O ₃ and LiAlO ₂	33
9. Particle Distribution Graphs of Al ₂ O ₃ and LiAlO ₂	33
10. Optical Microscope Images of Light Spent Fuel.....	34
11. Particle Distribution Graphs of Light Spent Fuel	34
12. SEM Images of Al ₂ O ₃ (spent fuel component)	35
13. SEM Images of Al(OH) ₃ (spent fuel component)	36
14. SEM Images of LiAlO ₂ spent fuel component)	37
15. SEM Images of LiOH (spent fuel component)	38
16. SEM-EDX Spectra of Spent Fuel (control)	39
17. SEM-EDX Spectra of Flow-Treated Spent Fuel	39
18. SEM-EDX Spectra of Hydrated Batch-Treated Spent Fuel	39
19. Normalized XRD Spectra of Spent Fuel and its Components	40
20. XRD Spectra Comparison of Different Industry Spent Fuel Samples	41
21. TGA Graph of LAH Thermolysis	44
22. TGA Graph of LiOH	45
23. TGA Graph of Al(OH) ₃	45
24. Initial Setup of Batch Synthesis Experiment	46
25. TiCl ₄ Bubbler Mass Flow Controller Calibration Curve.....	51
26. Water Bubbler Mass Flow Controller Calibration Curve	51

1. Introduction

A growing market for aerial drones in various public sector applications—such as infrastructure inspections, firefighting, search and rescue, and environmental monitoring—calls for the development of more resilient and reliable capability.¹ Traditional fuel cells may rely on energy sources such as hydrocarbons (e.g. natural gas) or pressurized gas that are too heavy for drones. Recognizing the need for an alternative and sustainable source of energy, current drone development has shifted towards hydrogen fuel cells.

Solid lithium aluminum hydride (LiAlH_4) can be used to generate hydrogen gas on demand using only water.² Water vapor and heat are generated as environmentally friendly byproducts. However, this chemical reaction presents safety challenges due to its highly exothermic nature. Coupled with the fuel's strong reducing-agent properties, LiAlH_4 's high reactivity may lead to thermal runaway and uncontrolled, unintended explosions. In addition to introducing operational difficulties, this is problematic for fuel cell disposal at the end of lifecycle due to the potential for unintended reaction during transit.

To try and mitigate these risks, the possibility of creating a passivating titanium oxide (TiO_2) coating using TiCl_4 is explored through batch and flow experimentation. TiO_2 bonded to the surface of LiAlH_4 , may create a protective shell. If experimental analyses deem sufficient titanium coverage on spent fuel surface as a potential passivating agent, further investigation involving in-flight fuel cell passivation during thermal runaway, or emergencies addressed by employing an on-demand surface passivation mechanism may be of high interest. Additionally, material characterization of spent fuel was conducted to better understand physical properties such as composition, surface chemistry, particle size distribution, and water retention.

1.1 Project Objectives

Our two main project objectives were to perform ex-situ spent fuel characterization before and after TiCl_4 surface coating to determine elemental composition, and to investigate the effectiveness of Titanium coating onto treated spent fuel in batch and flow.

2. Background

2.1 PEM Fuel Cell

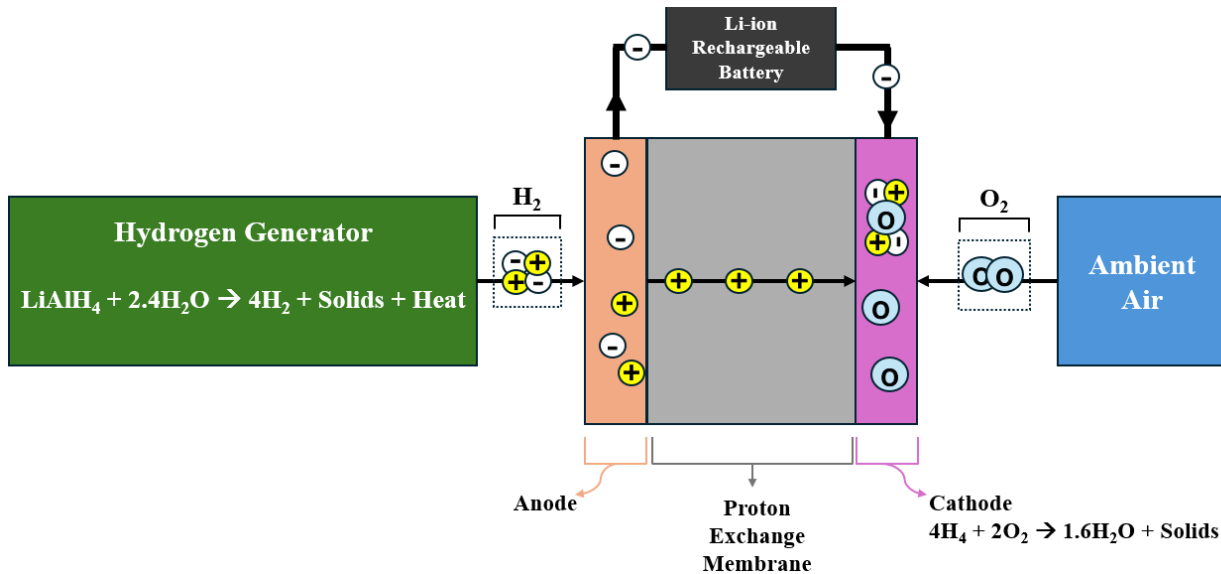


Figure 1. Operating principle of a solid-state fuel cell using hydrogen. Possible solid products in the hydrogen generator includes metal oxides and hydroxides.

A solid-state fuel cell (i.e. SSFC) is a cyclic process that produces electricity through an electrochemical reaction between the supplied fuel and an oxidizing agent.³ **Figure 1** demonstrates an SSFC operating with hydrogen as an oxidizing agent. Hydrogen ions act as fuel that travels through the proton exchange membrane (i.e. PEM) to be oxidized by oxygen in the cathode. The water can then be captured through an exhaust and reused in the hydrogen generator to synthesize more hydrogen.⁴

2.2 Metal Hydrides for Hydrogen Storage

For the use of drones in civil applications, a significant emphasis is placed on efficient energy or fuel storage—particularly for prolonged operational periods and when refueling or recharging the device on the field is not feasible. Among the various types of hydrogen storage methods, hydrogen fuel cell technologies currently offer an advantage with energy storage with maximum densities between 0.33 and 0.51 $\frac{kWh}{L}$.⁵ Metal hydrides have been emerging as a promising avenue enhancing hydrogen storage density.⁶ They also

provide flexibility in tailoring different thermodynamic properties for metal hydride-based hydrogen storage and supply systems based on parent material composition.⁶

2.2.1 Hydrogen Desorption Improvements with Titanium

Reversible hydrogen storage systems utilizing metal hydrides have been challenging to implement. Due to low rates of hydrogen desorption at low temperatures, adequate reaction rates are only obtained at temperatures of roughly 300 °C, which presents safety concerns since the desorption of hydrogen is highly exothermic (Bogdanović, 1997). To allow for adequate desorption rates at lower temperatures, Titanium compounds (TiCl_3 , $\text{Ti}(\text{O}-n\text{-C}_4\text{H}_9)_4$, and $\text{Ti}(\text{O}i\text{Bu})_4$) have been used as doping agents on the surface of metal aluminum hydrides (NaAlH_4 , Na_3AlH_6 , and $\text{Na}_2\text{LiAlH}_6$).⁷ Pressure-Composition Isotherms (PCI diagrams) were used to show pressure plateaus dependent on temperature for each metal aluminum hydride. For NaAlH_4 , two plateaus corresponding to the two reversible reactions that take place in the hydrogen desorption from sodium aluminum hydride.⁷ The first NaAlH_4 reversible dissociation happens at lower temperatures, while the second reversible dissociation happens at slightly higher temperatures. For Na_3AlH_6 and $\text{Na}_2\text{LiAlH}_6$ hydrogen desorption reactions, only one plateau was observed.⁷ Thermovolumetric curves for dehydrogenation showed that Ti-doping NaAlH_4 resulted in desorption 80-85 °C lower than NaAlH_4 that was undoped. By releasing more hydrogen at significantly lower temperatures, thermal runaway can be avoided.⁷

2.3 Lithium Aluminum Hydride

Table 1. A short list of LAH characteristics⁸

Molar Mass	Density	Melting Point	Initial Boiling Point	Structure
37.95 g/mol	920 kg/m ³	125 °C/257 °F	89-90 °C/192-194 °F	Tetrahedral

LiAlH_4 (i.e. Lithium Aluminum Hydride, Lithium Aluminate or LAH), a type of metal hydride, that is widely used in industry for its advantages in performance such as hydrogen release, purity, and storage.

Table 1 above lists a couple of LAH properties. LAH is a strong reagent that has versatile applications in organic synthesis, materials science, and inorganic chemistry, especially as a hydrogen source for various

chemical processes. LAH is a strong reducing agent as the aluminum is less electronegative while the Al-H bond is more polar. It is also known to reduce compounds such as carbonyls, nitro, amides, and epoxides as well as deoxygenate oxides (e.g., phosphine oxides and sulfoxides).⁸

LAH's application in PEM fuel cells is hindered due to various obstacles such as high dehydrogenation temperatures requirements, slow dehydrogenation kinetics, and reversibility issues. Complex metal oxide additives are an emerging research topic due to their property of enhancing dehydrogenation in metallic hydrides. A 2023 case study observed dehydrogenation temperatures—from two thermal events that occur in LAH—reduce from 146°C and 180°C to 92°C and 128°C after LAH was doped using TiSiO₄.⁹ The dehydrogenation kinetics were significantly improved with the titanium catalyst, improving the rate by 500%. The non-doped LAH sample had four thermal events in a range of 50 to 225 °C—two were exothermic and the others were endothermic. The Ti doped LAH thermal properties were reduced to two thermal events where one was exothermic, and the other was endothermic. This is most likely because the decomposition of the first stage was lower than the melting temperature of the non-doped sample. The activation energy also decreased significantly from 103 and 115 $\frac{kJ}{mol}$ to 68 and 77 $\frac{kJ}{mol}$.⁹ The reaction kinetics increased while the activation energy decreased because of decreased particle size. Decreasing the particle size increased the diffusion rate for hydrogen particles inside the fuel cell.⁹

2.3.1 Handling LAH

The pyrophoric chemical can be ordered in different forms depending on the intended use. A particular organic synthesis lab had three separate events where students mishandled the chemical due to a wrong order; LAH pellets were grinded inside a mortar and pestle instead of LAH powder.¹⁰ The grinding action inside the mortar supplied enough force to generate localized heat in the LAH, leading the material to reach its autoignition temperature of 125 °C. While this danger is emphasized by PubChem, the safety data sheet (Table 2) lacked this clarity, thus potentially causing confusion regarding whether grinding LAH posed a hazard.¹⁰

Several corrective actions were implemented following these incidents to prevent future incidents. Standard Operating Procedures (SOPs) were developed to ensure the safe handling of LAH. A protocol was established mandating the immediate reporting of near-miss incidents to the research advisor.¹⁰ Furthermore, a comprehensive Management of Change safety review was implemented to enhance overall safety protocols in the lab. These measures were put in place to mitigate risks and foster a safer working environment for all researchers involved. Due to safety concerns, this project investigated the passivation of fully reacted LAH (i.e. spent fuel) only. However, characterization tools were used to compare LAH to spent fuel and its known components—PhD student Januario Da Costa handled the LAH metal hydride for this project.

2.4 Surface Passivation

One method to avoid thermal runaway is surface passivation. Passivating the surface involves a process or treatment that is externally applied on a material's surface to protect it from environmental factors, especially since LAH is highly reactive to external water and most air. This method may also mitigate the risk of water molecules displacing inside the fuel during transport and potentially reacting with the surface. Because of previous literature using Titanium compounds as surface doping agents^{7,9}, it seemed promising to deposit titanium compounds as a surface coating layer to passivate the sample.

Hydride passivation is still a novel approach with limited literature on types of techniques. Bongso et al. (2022) investigated the strong chemical bond between LAH and TiCl_3 for the purpose of a McMurry coupling reaction.¹¹ Watson et al., (2023) highlighted the potential use of TiCl_3 to create an impermeable layer on the hydride surface.¹² TiCl_3 is commonly found in solution, making a passivation technique difficult to implement. TiCl_4 unless Cl_4 , however, is readily available as a volatile liquid, making surface passivation much more feasible.

A 2010 study investigated the kinetics of TiCl_4 hydrolysis.¹³ As such, gaseous TiO_2 may be able to coat the surface layer of the spent fuel through physisorption. TiO_2 has three phases—rutile, anatase, and brookite (rare). Vapor-phase TiCl_4 readily hydrolyzes (in the gas-phase) with ambient air at room temperature

to form TiO₂ nanoclusters [Equation 1].¹³ At room temperature (298K), TiO₂ is most thermodynamically stable in its rutile, polycrystalline form compared to pure anatase [Equation 2].¹³ Anatase-phase particles can still, however, form from having a lower reaction temperature. Anatase can thermally convert to the rutile phase between 700-800 °C.¹³



2.5 Spent Fuel Composition

When lithium aluminum hydride (LAH) undergoes hydrolysis, the desired reaction in the hydrogen generator, multiple solid byproducts are produced alongside the hydrogen gas with LAH reacting in the presence of water. These solid byproducts include lithium aluminate, lithium hydroxide, and aluminum hydroxide. At elevated temperatures, the undesired reaction in the generator, thermolysis, causes the decomposition of LAH into hydrogen, lithium, and aluminum. The industrial spent fuel sample is fully reacted LAH, containing a mixture of solid byproducts from the hydrolysis and thermolysis reactions. Passivation of the spent fuel's surface was tested in batch and flow scenarios.

2.6 Characterization Methods

2.6.1 DRIFTS

Diffuse Reflectance Infrared Fourier Transform Spectroscopy (DRIFTS) is a laboratory instrument that directly shines an infrared (IR) at a sample mixed with a transparent matrix.¹⁴ As the IR beam moves the sample, it reflects off the surface of the particles present, causing the light to diffuse. Subsequently, the diffused light exits the sample and is reflected off the output mirror onto the spectrometer's detector that then generates a spectrum illustrating sample composition.¹⁴ DRIFTS is particularly useful for the analysis of powders such as spent fuel. Surface analysis can be conducted to assess effectiveness of TiCl₄ passivation on the powder's outer layer. However, it's crucial to note that for powders to be effectively analyzed, they should be ground to a size of less than 10 microns. This recommendation brings up combustion concerns as previously mentioned

with grinding incidents using a mortar and pestle to reduce particle size.¹⁰ Thus, DRIFTS was not used to analyze LAH.

2.6.2 SEM-EDX

Scanning electron microscopy (SEM) is a material characterization technique that generates high magnification surface morphology images of a sample.¹⁵ In a vacuum environment (to prevent air molecules from interfering), SEM passes a focused beam of electrons over the sample surface. Multiple processes take place when the electron beam interacts with the sample. Ejections of secondary electrons from the sample surface may take place, which provides information on composition and surface features of the sample.¹⁵ Additionally, the intensity of backscattered electrons can tell us information on the sample material's atomic number, thus yielding contrast in the image. Characteristic X-rays may also be emitted as the high-energy electrons excite atoms in the sample; this carries information about elemental composition.

Energy-Dispersive X-ray Spectroscopy (EDX) is a complementary material characterization technique that is often used alongside SEM.¹⁵ EDX is primarily focused on obtaining information on a sample's chemical composition through elemental analysis. It analyzes the characteristic X-rays that the SEM produced to identify and quantify present elements in the sample.¹⁵ This is shown as a spectrum of compiled characteristic energy levels (i.e. peaks). SEM-EDX is critical in assessing the extent of Titanium presence on spent fuel from TiO₂ coating.

2.6.3 XRF

X-Ray Fluorescence (XRF) spectroscopy is another type of elemental analysis that measures fluorescent x-rays emitted by the tested sample from a primary x-ray source.¹⁶ The emitted x-rays are diffracted differently depending on the type of element present, thus gathering information on different weight percentages of metals in the sample. Using a Bruker Countertop XRF Analyzer (CTX), surface analysis can be performed to obtain the weight percent of metals present on the outer layer of the sample.¹⁶ Results from

this instrument were used as a secondary source to verify surface composition data that the SEM-EDX collected.

2.6.4 Raman Spectroscopy

Raman spectroscopy is a non-destructive means of analysis that provides detailed information on chemical structure, phase, polymorphy, crystallinity, and molecular interactions.¹⁷ This method uses light scattering techniques and sensing to match documented spectra of potential chemical species in the sample. Raman may help give insight on which chemical compounds are present during different stages of the metal hydride fuel (i.e. LAH, spent fuel, spent fuel after batch, and spent fuel after flow).

3. Methods

3.1 Materials

Experimentation on spent fuel also involved characterization of its separated, expected components: Alumina, Aluminum Hydroxide, Lithium Aluminate, and Lithium Hydroxide. Chemical agents were stored in a fume hood inside a desiccator. **Table 2** below briefly lists the chemical compounds used in this project.

Table 2. A summarized list of chemical agents used for experimentation. Safety data sheets for chemicals obtained from Sigma Aldrich are hyperlinked in the table. “RT” refers to room temperature. Lithium Aluminum Hydride was not handled by undergraduate students.

Compound	Properties	Safety Concerns
Alumina (Al ₂ O ₃)	White powder; combustible	Not a hazardous substance Store in appropriate ventilation
Aluminum Hydroxide (Al(OH) ₃)	White solid; not combustible	Not a hazardous substance Store in appropriate ventilation
Lithium Aluminate (LiAlO ₂)	Powder; chemically stable under ambient conditions	Causes skin irritation May cause respiratory irritation
Lithium Hydroxide (LiOH)	Crystalline; chemically stable under ambient conditions	Causes severe skin burns and eye damage
Lithium Hydroxide (LiOH)	Crystalline; chemically stable under ambient conditions	Causes severe skin burns and eye damage

3.2 Synthesis of Titanium Coating Experimentation

3.2.1 Reagent Preparation

The spent fuel samples were dried in an oven for at least 2 days prior to experimentation to evaporate away residuals such as excess water. Approximately 0.5 g of spent fuel was used in each trial (batch & flow). Liquid TiCl₄ was drawn into a syringe in argon in a glove bag. After injection, syringes were left under the fume hood to let the TiCl₄ inside completely react before being discarded.

3.2.2 System Preparation

Before each run, all relevant equipment (e.g. stoppers, flasks, vials, idex fittings) were cleaned and then dried in the oven. Additionally, the reactor vessels were purged with Argon gas for 20-25 minutes before every run to remove air and excess moisture in the system.

3.2.3 Batch Reactor Experiment

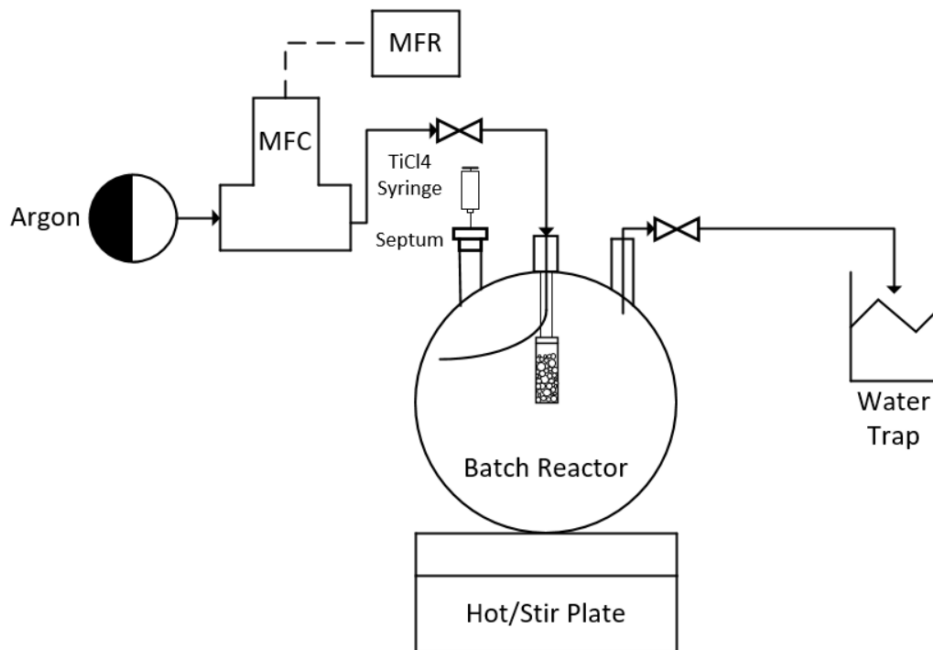


Figure 2. Flow diagram of Batch Reactor apparatus in the fume hood (with sand bath illustration excluded).

The batch reactor consists of a 1L three-necked round bottom flask in a sand bath atop a hot plate (see **Figure 2**). Two necks were sealed using rubber stoppers— PFA tubing is inserted in each rubber stopper for gas flow. The third neck was sealed with a rubber septum for injecting TiCl_4 into the system. The spent fuel sample was suspended in a glass dram vial using a harness tied with PFA tubing. The vial was hung from the central rubber stopper. A previous iteration of the experiment used a plastic cuvette, which reacted with the reactor environment (**Appendix B**).

Two experiments were performed with the batch reactor. The aim of the first batch experiment was to observe if TiCl_4 vapor reacts with spent fuel alone. In the second experiment, water was pre-loaded onto the spent fuel. 0.2 mL of water was injected onto the spent fuel sample prior to the addition of TiCl_4 . 0.2 mL of TiCl_4 was injected into the flask after argon purging. As the reaction produces HCl gas the outlet stream was left open during the reaction to prevent pressure buildup. Dry and hydrated trials were compared to see if water on the spent fuel's surface improved Titanium coating as opposed to solely relying on gas hydrolysis

with ambient air. DRIFTS, SEM-EDX, Raman Spectroscopy, and XRF were performed on samples before and after the batch reaction to characterize the surface of the material and determine if a titanium layer had been deposited on the surface of the spent fuel.

3.2.4 Packed Bed Reactor Experiment

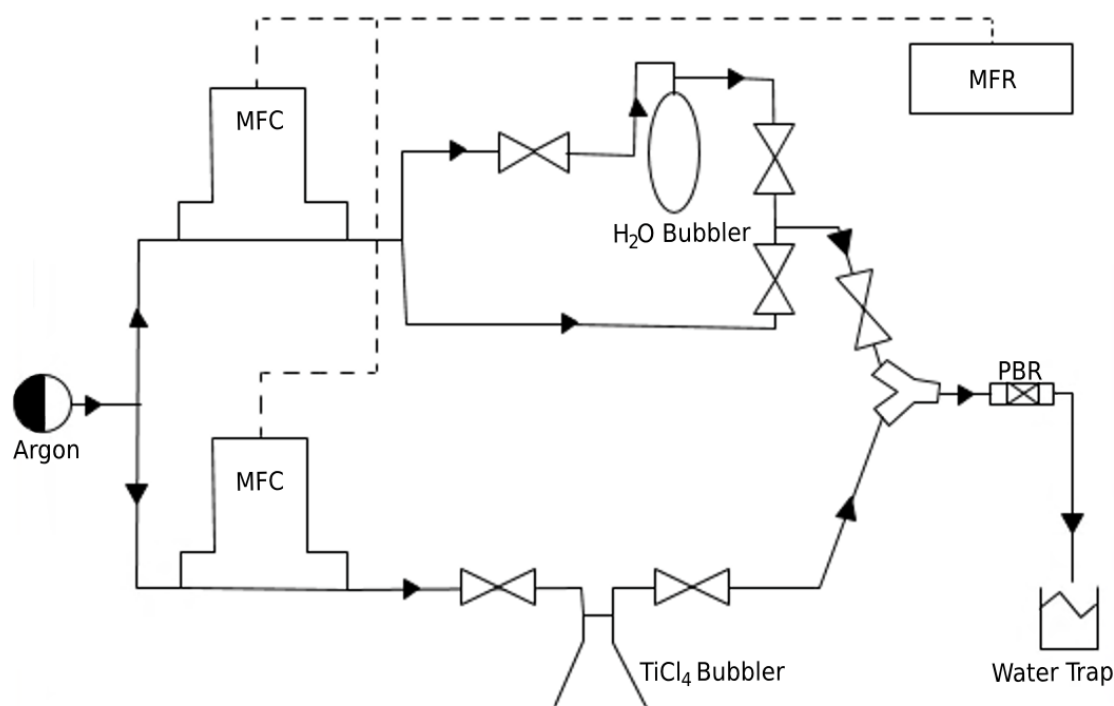


Figure 3. P&ID of flow-cell experiment with Spent fuel and TiCl₄.

The packed bed reactor (PBR) was used to humidify a spent fuel sample, then expose it to TiCl₄ vapor in flow. In the design, two mass flow controllers (MFCs) are used to measure and control the flow of argon gas. One MFC is used to provide gas to a water bubbler and a dry argon line, while another is used to control the mass of gas passing through the TiCl₄ bubbler. The two MFCs were connected to a mass flow reader (MFR), which operated the MFCs and displayed the flowrate. The fritted water bubbler uses a stainless-steel body and 2 mm HPLC filter. Due to its incompatibility with metal, a 25 mL Erlenmeyer flask capped with a rubber stopper serves as the TiCl₄ bubbler. PFA tubing passes through the rubber stopper to provide an inlet and outlet. Rather than a metal frit, a 0.4 mm capillary tube is inserted into the end of the PFA

tubing to limit the size of the gas bubbles passing through the liquid TiCl_4 . Gas flow rates were determined with MFC calibration curves constructed using a bubble meter (**Appendix C.4**).

The PBR body is constructed out of a 6 cm length PEEK tubing and sealed with flangeless fittings. The gas which passes through the PBR then flows into a beaker full of water to react any unreacted or partially reacted TiCl_4 and absorb HCl gas. The PBR would then be saturated by the water bubbler for 20 minutes at a rate of 1.38 mL/s. Gas bubbled through the TiCl_4 was then flowed through the PBR at a rate of 1.30 mL/s for 5 minutes.

3.3 Preparing for Characterization

SEM with EDX was used to collect images and create an elemental distribution map of the spent fuel surface before and after TiCl_4 treatment. Data was collected for reference materials purchased from Sigma-Aldrich, an untreated spent fuel sample, and spent fuel samples treated with TiCl_4 in a batch and flow apparatus. DRIFTS was performed on spent fuel before and after bench scale passivation to analyze surface chemistry for evidence of a passivation layer on the sample. Spent fuel was ground in a mortar and pestle optimal analysis before running DRIFTS pre-passivation. After bench scale passivation, the sample was run in DRIFTS to look for evidence of TiO_2 layer(s) caused by the reaction of TiCl_4 with water in our bench scale apparatus. Each sample in DRIFTS was about 10 mg, and the experiment was run in a Nitrogen environment within the DRIFTS cell.

4. Results and Discussion

4.1 Batch and Flow TiCl_4 Coating Experiments

Titanium containing compounds were successfully deposited onto the surface of spent fuel samples in both batch and flow. The presence of titanium on these samples was confirmed with SEM EDX and XRF. Additionally, a mass balance on the flow-coated spent fuel sample shows mass gain more than the mass of the water exposed to the sample. Evidence of residual water on both coated and uncoated spent fuel was found with DRIFTS and Raman spectroscopy.

Due to flaws in the experimental setup, significant portions of the coated batch samples were spilled and lost. Additionally, while the dry batch experiment did not have any water added to the system, the argon purge was incomplete, and the hydrolysis of TiCl_4 was still observed. The batch apparatus was useful in providing another data point to show that TiCl_4 can indeed be used to coat samples and was easier to set up, but it was inconsistent to operate. Mass balance could not be performed due to sample spillage.

Theoretical maximum mass gain of a sample exposed to TiCl_4 vapor in flow was calculated assuming saturated vapor was exiting the TiCl_4 bubbler (**Appendix C.2**). Vapor pressures were calculated using Antoine's equation and moles of substance from the ideal gas law (**Appendix C.1**). The total mass of TiO_2 which could be generated by argon vapor saturated in TiCl_4 flowing at 1.3 ml/s for five minutes was calculated to be 49.1 mg. The water sorption of a spent fuel sample was measured by flowing water over a spent fuel sample in flow and measuring the mass gain (**Appendix C.3**). From this testing, we would expect between 1.0 ~ 4.0 wt% water content on the sample after exposure to water vapor at 1.38 ml/s for twenty minutes. With an initial sample mass of 474.6 mg, the anticipated water uptake would be 19.0 mg. The measured mass difference before and after experimentation in the spent fuel sample was 29.4 mg. This exceeds the mass which would be gained simply by water, suggesting that there was more than 10 mg of TiCl_4 hydrolysis products deposited onto to the sample.

Gas leaks across the Swagelok joints of the water bubbler were a consistent issue during the development and operation of the flow apparatus. This led to large inconsistencies in the measured data for water uptake of the sample. Leakage of water vapor as well as non-equilibrium conditions in the TiCl_4 and water bubblers result in smaller amounts of vapor reaching the sample than estimated. This makes the resulting yield greater than it may initially appear. Residual water was also present in the gas lines of the apparatus leading up to the sample due to the shared line after the merging y, resulting in some premature hydrolysis of the TiCl_4 . Small diameter tubing was also observed to be prone to buildup of products of TiCl_4 hydrolysis, leading to increased pressure drop through the system.

The exact composition of the products of this reaction were not identified. While titania is the product of complete hydrolysis of TiCl_4 , titanium hydroxide, and other intermediates are also potential products of the reaction. Exactly which products were generated, and in what ratios, could be explored. Additionally, greater exposure times to both TiCl_4 and water could lead to more consistent results. Varying exposure time could also give greater insight into the development of a layer on the surface of the spent fuel.

4.2 Spent Fuel Characterization

4.2.1 SEM-EDX

SEM-EDX is critical in assessing the extent of Titanium presence on spent fuel from TiO_2 coating. SEM images of spent fuel, as received, and after treatment with TiCl_4 are shown in **Figure 4** on the next page. Elemental distribution images show the composition of the surfaces of the respected samples that we analyzed using this method. Oxygen, aluminum, titanium, and chlorine were identified. Due to its small size SEM-EDX could not measure lithium. EDX of the as-received spent fuel shows that aluminum and oxygen are evenly distributed throughout the surface of untreated spent fuel (**Figure 4**). EDX of the treated spent fuel shows chlorine and titanium on the surface of the spent fuel, in addition to aluminum. Oxygen was excluded from these images for clarity. However, rather than forming a uniform coating, the titanium did not deposit onto the entire surface evenly. In both flow and hydrated batch trials, titanium forms a sporadic coat onto the

surface of the particles. Particularly in image B, regions of less dense titanium content, and other, larger clusters of titanium are visible. Other surfaces do not read as having any titanium, and only aluminum and oxygen.

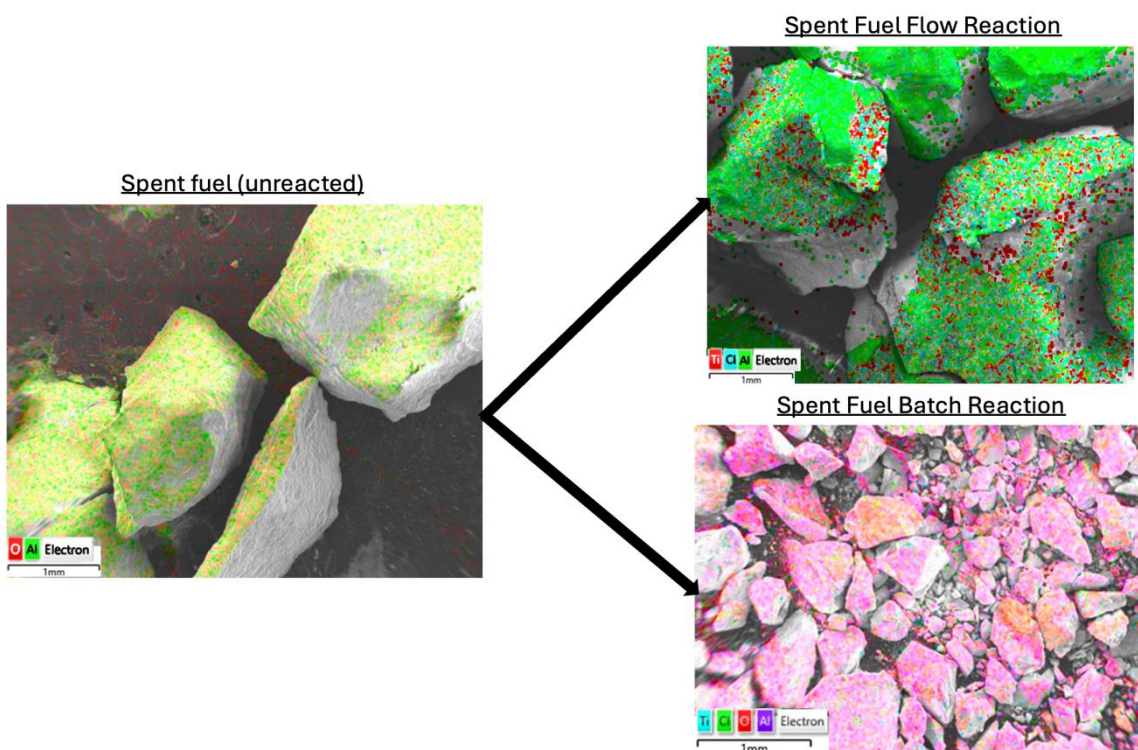


Figure 4. Images generated with SEM/EDX on spent fuel samples. Industry spent fuel (left) shows no titanium content. Spent fuel treated with TiCl_4 in flow (top right) shows titanium deposited in red. Ground spent fuel after TiCl_4 exposure in the batch reactor (bottom right) shows titanium (teal).

Despite TiCl_4 being in excess in the batch reactor compared to the excess of water in flow, as well as the batch setup having a higher exposure time than the flow setup, more titanium coated the surface in flow than in batch. This indicates that the flow apparatus was more effective in coating the spent fuel than the batch apparatus. In the flow apparatus, all the TiCl_4 vapor generated was forced to pass through the packed bed, and all the spent fuel before exiting the system. This contrasts with the batch apparatus, where the sample was simply suspended in an environment of largely stagnant vapor. This difference is a likely contributing factor to the greater amount of titanium observed on the flow sample.

There is a possibility that TiCl_4 completely reacted to where the water is. However, we were not able to run an SEM analysis on a sample that had only water flow over it. If we did have a run measuring water, we would be able to see oxygen on the surface from physisorbed water in SEM-EDX images. TiCl_4 's effectiveness in coating the spent fuel with a layer of titania could be evaluated by varying the amount of water present on the surface before the reaction takes place, then varying the flow and/or time that TiCl_4 flows through the PBR. Maximizing Ti-coating to create a passivation layer can be achieved by optimizing flow rate for TiCl_4 as well as time for TiCl_4 flow through the PBR.

4.2.2 X-Ray Fluorescence Spectroscopy

XRF measured the samples' weight percent of metals detected on the surface. **Figure 5** on the next page displays weight percent readings from received spent fuel (A), TiCl_4 -treated spent fuel in flow (B), and TiCl_4 -treated spent fuel in batch (C & D). Some unexpected metals were present in the results such as Silicon (Si), Palladium (Pd), Tellurium (Te), and Iron (Fe). The team has not identified the source of error; it is possible that the material tray was contaminated during spectra readings or there was an insufficient background run to remove noise, thus leading to skewed weight percentages.

Nevertheless, we were able to verify Titanium presence on the surface from both batch and flow treatments that the SEM-EDX identified. Titania coating was notably more successful in the flow experimentation, with its surface displaying the highest weight percentage of 34%, relatively. This observation aligns with SEM-EDX spectra results (see **Appendix A.3**), which show a higher presence of Titanium peaks on the surface under flow conditions.

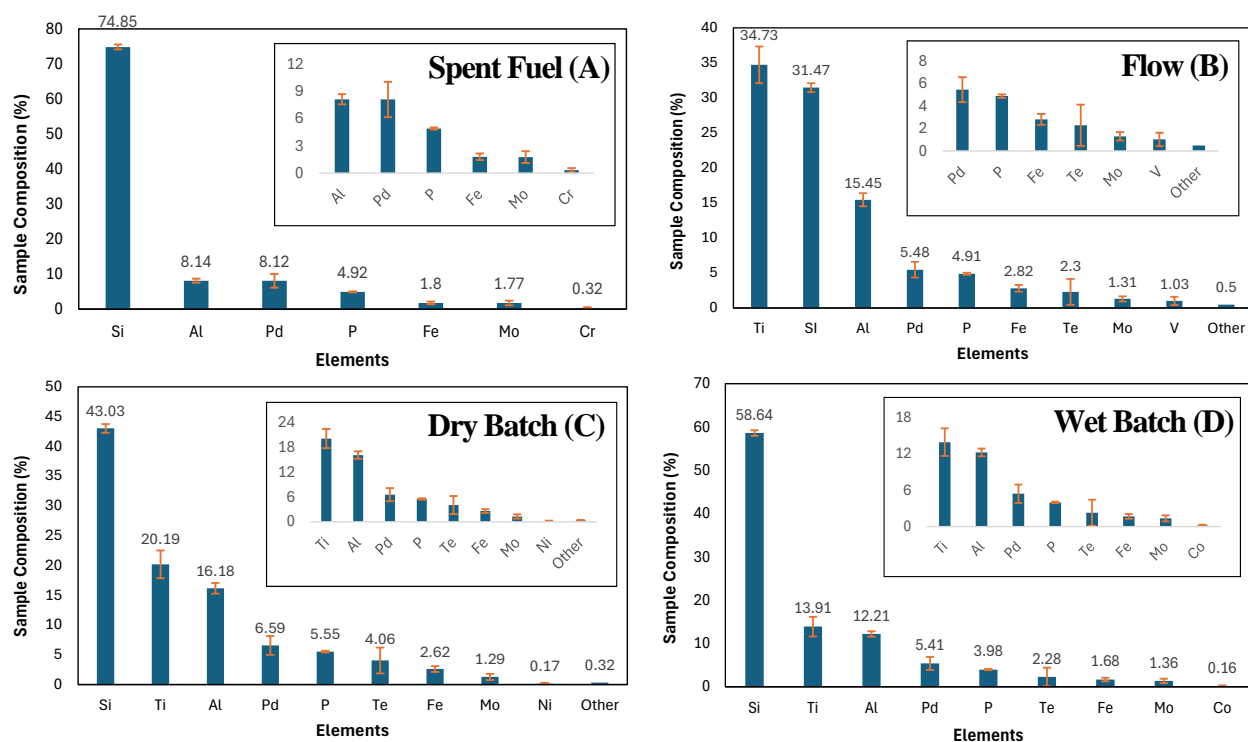


Figure 5. XRF-generated weight percent of metals present on the surface of spent fuel samples that undergone synthesis experimentations: A) spent fuel, B) flow, C) dry batch, and D) wet batch.

Another notable element detected was Silicon (Si). Si is not among the initially expected components, which includes LiOH , Al_2O_3 , LiAlO_2 , and $\text{Al}(\text{OH})_3$. While small traces of silicon may have been introduced into the spent fuel sample, it is unlikely that this alone could account for the significant weight percentage detected by XRF. The presence of silicon was also not observed with EDX. There may be Si peaks that have not yet been conclusively identified in the Raman spectroscopy (see **Figure 6** on the next page). Further characterization will be needed to confidently rule out silicon. If there is significant silicon presence on the surface of the spent fuel, it is necessary to investigate the passivation's chemical process to determine whether TiO_2 is solely physisorbed onto the surface, or if there is chemisorption of Si-O bonds on the surface that contributes to adhesion and stability of the passivation.

4.3.3 Raman Spectroscopy

Figure 6 below displays normalized spectra for peak comparison to look for any Titania compounds. It was difficult to determine which oxides comprised most of the industry spent fuel in the Raman—XRD analysis in **Appendix A.4** points towards LiAlO_2 and Al_2O_3 as most prominent within the spent fuel sample. It should be noted for Raman that there are some data spikes—sharp peaks not sharp bands—throughout the spectra (such as those near 1250 cm^{-1} and 3000 cm^{-1}). These outliers can be caused by several factors including sample impurities and resonance Raman scattering. To present the complete data set, these spikes were not removed. If necessary, they can be removed using a modified Z-scores outlier detection-based algorithm.¹⁸ **Table 3** on the next page lists all the potential peak modes that have currently been identified.

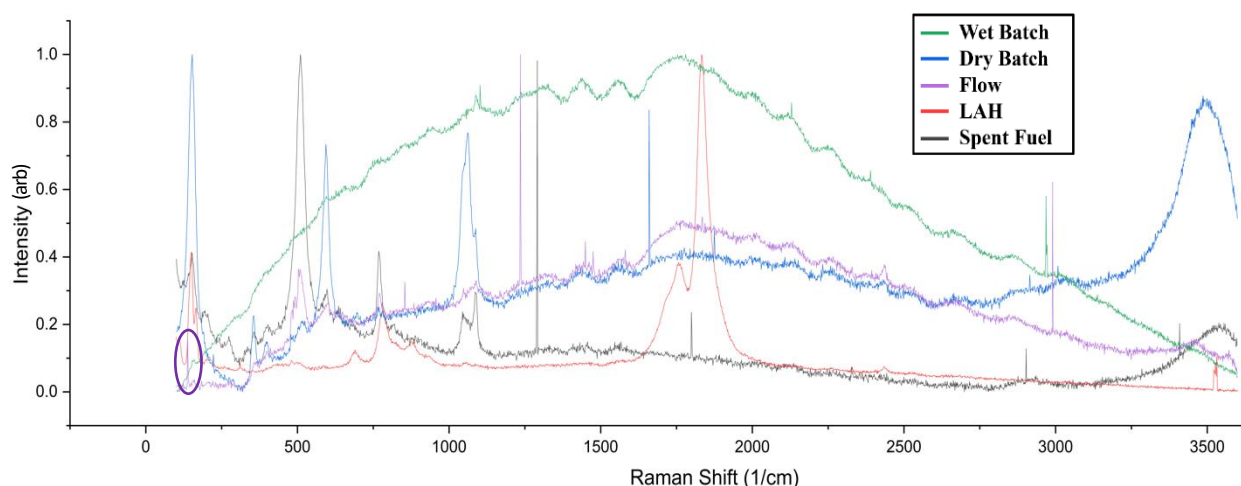


Figure 6. Normalized Raman Spectroscopy data on spent fuel (gray), Lithium Aluminum Hydride (red), flow treatment spent fuel (purple), dry batch treatment spent fuel (blue), and wet batch treatment spent fuel (green). The purple peak circled on the bottom left potentially identifies TiO_2 presence in the flow-treated sample.

For future experimentation, samples should be dried for a longer period to remove noise from excess water molecules. There were, however, still some peaks visible enough to read—LAH (orange in **Figure 6**) presented peak frequencies that corroborate with literature values.¹⁹ When compared to the other samples, it is apparent that many of the LAH components have reacted. There are some remnants of Al-H bonds around

800 cm^{-1} that are present in all the other samples (inconclusive for the wet batch). As expected, the dry batch reacted the least since TiCl_4 cannot effectively hydrolyze to form TiO_2 without enough water (gray).

The most notable peak (circled) on the graph is a thin, sharp-band at approximately 138 cm^{-1} that potentially identifies as TiO_2 .²⁴ This visible peak supports both SEM-EDX imaging as well as XRF weight percentages that indicate the flow-treated spent fuel having the largest titania presence. This peak resembles TiO_2 in the anatase phase²⁴ and not rutile phase²⁵. Because the reaction was not heated, the anatase-phase particles did not achieve the thermal conversion needed for stability. It is unknown if the physisorbed titania coating is robust enough to passivate the spent fuel surface without further experimentation.

Table 3. Potential Peak Identifications of Raman Spectroscopy shown in **Figure 6**.

Compound	Mode Frequency (cm^{-1})	Mode Description	Comments
LAH (orange)	149 and 164	Translation ¹⁹	
	689-937	Al-H bending ¹⁹	
	1720-1834	Al-H stretching ¹⁹	
Spent Fuel (gray)	508	Al-O bending ²⁰	
	656-827	Al-H bending ¹⁹	
	1084	LiOH ²¹	Right shoulder peak
	1400-1600	Al-H ²²	Double peaks
	3500	O-H ²³	
Flow (purple)	138	TiO_2 ²⁴	
	772	Al-H bending ¹⁹	
	1090	LiOH ²¹	Right shoulder peak
	1400-1600	Al-H ²²	Double peaks
Dry Batch (blue)	690-915	Al-H bending ¹⁹	
	1083	LiOH ²¹	Right shoulder peak
	1400-1600	Al-H ²²	Double peaks
	3500	O-H ²³	
Wet Batch (green)	1102	LiOH ²¹	Right shoulder peak
	1400-1600	Al-H ²²	Double peaks

4.3.4 DRIFTS

DRIFTS was performed at room temperature. Interestingly, for both spent fuel (A) and hydrated batch (B) samples, peaks near 3500 cm^{-1} indicate an O-H stretch on the surface of each sample (see **Figure 7**). For the spent fuel (control), this is likely indicative of residual water on the surface of the sample. There was not a significant decrease in absorbance at this peak from room temperature to $150\text{ }^{\circ}\text{C}$, but when the sample was heated to $250\text{ }^{\circ}\text{C}$, the absorbance decreased to roughly 50% of the absorbance at room temperature. Once the sample was heated to $400\text{ }^{\circ}\text{C}$, the absorbance at 3500 cm^{-1} was near zero, indicating water on the surface had fully evaporated. The spent fuel sample, despite being placed in an oven for 2 days to dry out, still has residual water present on the surface of the fuel, indicating that the spent fuel is very hygroscopic.

For the hydrated batch sample (B) in **Figure 7**, the absorbance at 3500 decreased slightly as temperature was increased from room temperature to $100\text{ }^{\circ}\text{C}$; once the temperature had reached $200\text{ }^{\circ}\text{C}$, the absorbance data began to fluctuate in absorbance from 3600 to 3200 cm^{-1} . From 300 to $500\text{ }^{\circ}\text{C}$, the OH peak absorbance went to near zero. The lower absorbance at 3500 cm^{-1} as temperature rose indicates that water on the surface present at room temperature evaporated as the temperature increased. This could potentially indicate $\text{Ti}(\text{OH})_4$ on the surface, but since our batch experiment had an excess of water (4:1 H_2O to TiCl_4), this is most likely a combination of $\text{Ti}(\text{OH})_4$ (if present) and H_2O . If this is the case, water or $\text{Ti}(\text{OH})_4$ on the surface could have reacted with the nitrogen flowing through the cell, causing the variance in absorbance from 3600 to 3200 cm^{-1} at $200\text{ }^{\circ}\text{C}$.

For both spent fuel (A) and hydrated batch (B) samples, multiple shouldering peaks are present between 1400 and 1700 cm^{-1} . For the spent fuel (A), the relative absorbance from room temperature to $250\text{ }^{\circ}\text{C}$ is consistent; a large decrease is present once heated to $300\text{ }^{\circ}\text{C}$. For the hydrated batch (B), the relative absorbance is consistent from room temperature to $100\text{ }^{\circ}\text{C}$, but once heated to $200\text{ }^{\circ}\text{C}$, the relative absorbance at 1640 cm^{-1} decreased significantly, while the relative absorbance at 1460 cm^{-1} went to near zero. Once the

sample had been cooled back down to room temperature, the absorbance at 1640, 1500, and 1430 cm^{-1} increased back to the pre-heating level.

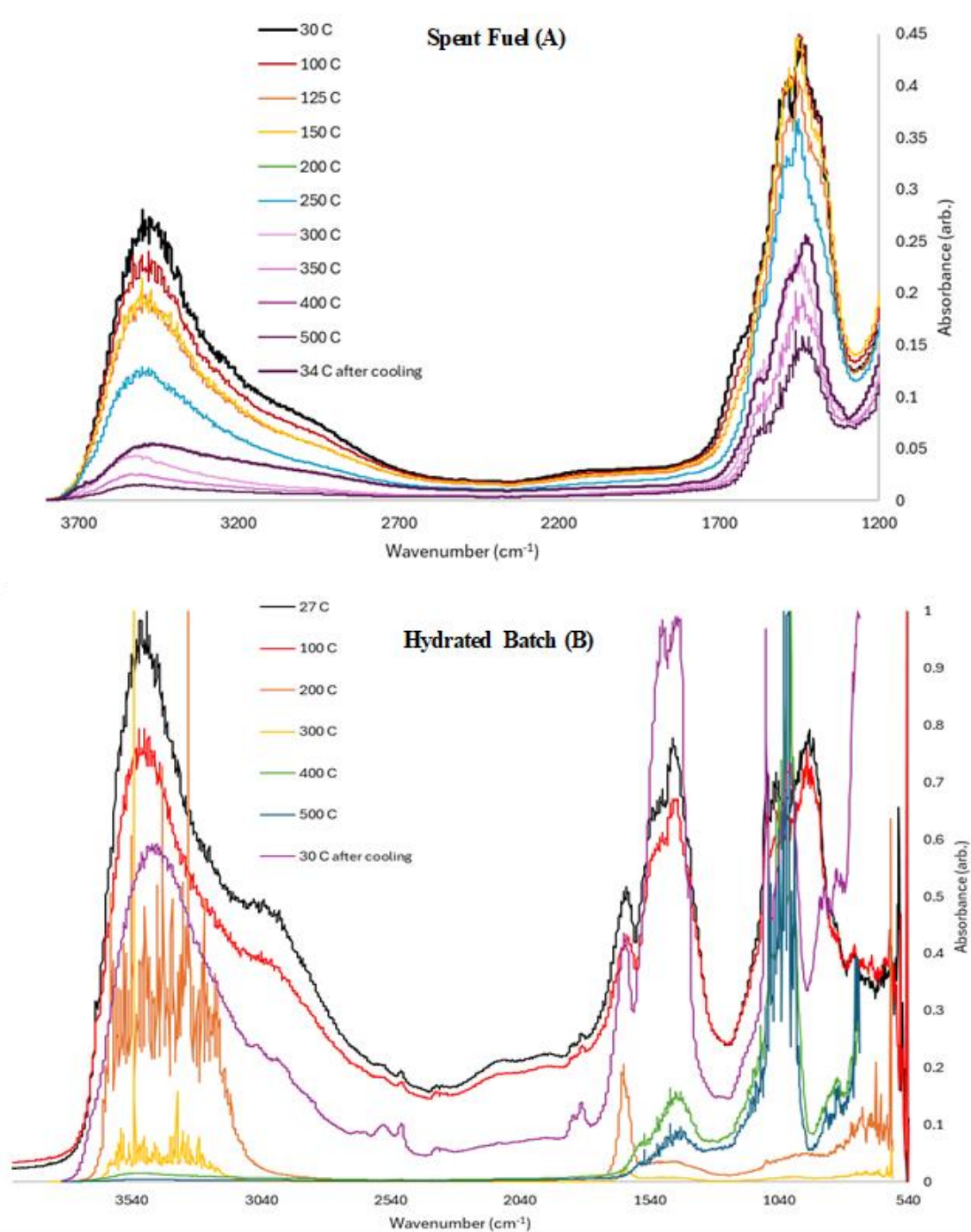


Figure 7. DRIFTS spectra for the A) spent fuel sample (control) from 30-500 °C and B) the hydrated batch experiment spent fuel sample from 27-500 °C

5. Conclusion & Recommendation

The key conclusions from the research are as follows:

- DRIFTS demonstrated that significant amounts of water are trapped within spent fuel until in excess of 300 °C
- TiCl_4 hydrolysis products can be deposited onto the surface of spent fuel in a flow cell

The potential for a runaway thermolysis reaction of LiAlH_4 poses a significant process safety issue. Particularly in vehicular applications, transport and storage of such a highly reactive fuel exemplifies a challenge. This project attempted to discover a potential method of surface passivation to improve safety of hydrogen fuel cell operation. To understand reaction dynamics and to better understand how reacted LiAlH_4 would interact with our method of passivation, industry spent fuel was characterized using multiple tools to understand chemical composition. XRD results (**Appendix A.4**) indicate that its primary oxides mostly consist of LiAlO_2 and Al_2O_3 . Titanium containing compounds were observed on the surface of spent fuel with SEM/EDX and confirmed with XRF after synthesis experiments—titanium presence was most prominent after flow treatment. However, the exact identity of these compounds was not identified. Raman Spectroscopy had an interesting peak in the flow spectra that may indicate TiO_2 but further analysis is required. Using DRIFTS, it was seen that while being fully reacted, the spent fuel still holds significant amounts of water internally, regardless of several days of moderate drying. This further confirms that spent fuel transportation is a concern. Simple drying of the spent fuel at low temperatures will not be an effective solution to guarantee its stability. DRIFTS also showed that in the short term, significant amounts of water wouldn't evaporate until reaching high temperatures of about 300°C. TiCl_4 was reacted on the surface of spent fuel. Aside from difficulties with the experimental apparatus, buildup of TiCl_4 hydrolysis products and clogging were identified as potential issues for TiCl_4 as a passivation solution.

In the short term we recommend trying to create a complete, enveloping layer on the surface of the spent fuel and determining whether it is enough to passivate the surface. While the reaction is effective at

scavenging water, it is unclear the degree to which a layer of TiO_2 would passivate a fuel cell. The interaction of HCl with the spent fuel is also an object of interest. Varying the time exposed to water vapor, TiCl_4 exposure, and packing amount could all be of interest. Additionally, the pressure buildup and accumulation of TiCl_4 hydrolysis products could also be investigated to understand how it could be more evenly distributed and stopped from accumulating problematically. Obtaining particle distribution (see **Appendix A.1**) of spent fuel samples using more SEM images (see **Appendix A.2**) would help in identifying surface porosity characteristics and how passivation will affect this. A more complete TGA analysis could also be performed to obtain more data on the thermolysis reaction of the fuel and spent fuel (**Appendix A.5**).

It is unclear whether this method of surface passivation with TiCl_4 is feasible. While the potential benefits of this method are great, it also introduces other concerns, such as HCl gas, and heat release from the reaction. Due to the great uncertainty associated with TiCl_4 passivation we would recommend investigating other methods of managing process safety concerns before further pursuing it.

6. References

- [1] Otto, A., Agatz, N., Campbell, J., Golden, B., & Pesch, E. (2018). Optimization approaches for civil applications of unmanned aerial vehicles (UAVs) or aerial drones: A survey. *Networks*, 72(4), 411–458. <https://doi.org/10.1002/net.21818>
- [2] Sazelee, N. A., & Ismail, M. (2021). Recent advances in catalyst-enhanced LiAlH₄ for solid-state hydrogen storage: A review. *International Journal of Hydrogen Energy*, 46(13), 9123–9141. <https://doi.org/10.1016/j.ijhydene.2020.12.208>
- [3] Singhal, S. (2000). Advances in solid oxide fuel cell technology. *Solid State Ionics*, 135(1-4), 305–313. [https://doi.org/10.1016/s0167-2738\(00\)00452-5](https://doi.org/10.1016/s0167-2738(00)00452-5)
- [4] Lototsky, M. v., Tolj, I., Pickering, L., Sita, C., Barbir, F., & Yartys, V. (2017). The use of metal hydrides in fuel cell applications. In *Progress in Natural Science: Materials International* (Vol. 27, Issue 1). <https://doi.org/10.1016/j.pnsc.2017.01.008>
- [5] Andrews, J., & Shabani, B. (2012). Re-envisioning the role of hydrogen in a sustainable energy economy. *International Journal of Hydrogen Energy*, 37(2), 1184–1203. <https://doi.org/10.1016/j.ijhydene.2011.09.137>
- [6] Bellosta von Colbe, J., Ares, J.-R., Barale, J., Baricco, M., Buckley, C., Capurso, G., Gallandat, N., Grant, D. M., Guzik, M. N., Jacob, I., Jensen, E. H., Jensen, T., Jepsen, J., Klassen, T., Lototsky, M. V., Manickam, K., Montone, A., Puszkiel, J., Sartori, S., & Sheppard, D. A. (2019). Application of hydrides in hydrogen storage and compression: Achievements, outlook and perspectives. *International Journal of Hydrogen Energy*, 44(15), 7780–7808. <https://doi.org/10.1016/j.ijhydene.2019.01.104>
- [7] Bogdanović, B., & Schwickardi, M. (1997). Ti-doped alkali metal aluminium hydrides as potential novel reversible hydrogen storage materials. *Journal of Alloys and Compounds*, 253–254. [https://doi.org/10.1016/S0925-8388\(96\)03049-6](https://doi.org/10.1016/S0925-8388(96)03049-6)
- [8] *Lithium Aluminium Hydride- LiAlH₄ - Definition, Structure of lithium aluminium hydride, Properties, and Uses with FAQs.* (n.d.). BYJUS. <https://byjus.com/chemistry/lithium-aluminium-hydride/>
- [9] Yusnizam, N. Y., Ali, N. A., Sazelee, N., & Ismail, M. (2023). Boosting the Dehydrogenation Properties of LiAlH₄ by Addition of TiSiO₄. *Materials*, 16(6). <https://doi.org/10.3390/ma16062178>
- [10] Merlic, C. A., Ferber, C. J., & Schröder, I. (2022). Lessons Learned-Lithium Aluminum Hydride Fires. *ACS Chemical Health and Safety*, 29(4). <https://doi.org/10.1021/acs.chas.2c00035>
- [11] Bongso, A., Roswanda, R., & Maolana Syah, Y. (2022). Recent advances of carbonyl olefination via McMurry coupling reaction. *RSC Advances*, 12(25), 15885–15909. <https://doi.org/10.1039/D2RA00724J>

- [12] Watson, M., Soden, K., & Calistra, A. (2023). Surface Passivation of Hydride Fuel Cell for Process Safety. *Worcester Polytechnic Institute*.
https://digital.wpi.edu/concern/student_works/ks65hg73g?locale=en
- [13] Wang, T.-H., Navarrete-López, A. M., Li, S., Dixon, D. A., & Gole, J. L. (2010). Hydrolysis of TiCl_4 : Initial Steps in the Production of TiO_2 . *The Journal of Physical Chemistry A*, 114(28), 7561–7570.
<https://doi.org/10.1021/jp102020h>
- [14] Mitchell, Mark B. “Fundamentals and Applications of Diffuse Reflectance Infrared Fourier Transform (DRIFT) Spectroscopy.” *Advances in Chemistry*, 5 May 1993, pp. 351–375,
<https://doi.org/10.1021/ba-1993-0236.ch013>.
- [15] rmladmin. “Difference between SEM and EDX Analysis.” *Rocky Mountain Labs*, 20 Nov. 2023, rockymountainlabs.com/sem-and-edx-analysis/#:~:text=SEM%20is%20focused%20on%20providing.
- [16] “What Is Raman Spectroscopy? - HORIBA.” *Www.horiba.com*, www.horiba.com/int/scientific/technologies/raman-imaging-and-spectroscopy/raman-spectroscopy/#:~:text=Raman%20spectroscopy%20is%20a%20non.
- [17] “XRF Spectrometers.” *Www.bruker.com*, www.bruker.com/en/products-and-solutions/elemental-analyzers/xrf-spectrometers.html.
- [18] Coca, N. (2019, November 19). *Removing Spikes from Raman Spectra with Anomaly Detection*. Medium. <https://towardsdatascience.com/removing-spikes-from-raman-spectra-8a9fdda0ac22>
- [19] Chellappa, R. S., Chandra, D., Gramsch, S. A., Hemley, R. J., Lin, J.-F., & Song, Y. (2006). Pressure-Induced Phase Transformations in LiAlH_4 . *The Journal of Physical Chemistry B*, 110(23), 11088–11097. <https://doi.org/10.1021/jp060473d>
- [20] Hu, Q., Lei, L., Jiang, X., Zhe Chuan Feng, Tang, M., & He, D. (2014). Li ion diffusion in LiAlO_2 investigated by Raman spectroscopy. *Solid State Sciences*, 37, 103–107.
<https://doi.org/10.1016/j.solidstatesciences.2014.08.017>
- [21] Gorelik, V. S., Bi, D., Voinov, Y. P., Vodchits, A. I., Gorshunov, B. P., Yurasov, N. I., & Yurasova, I. I. (2017). Raman spectra of lithium compounds. *Journal of Physics. Conference Series*, 918, 012035–012035. <https://doi.org/10.1088/1742-6596/918/1/012035>
- [22] Jean-Claude Burcau, Amri, Z., Claudy, P., & Jean-Marie Létoffé. (1989). Etude comparative des hexahydrido- et des hexadeuteridoaluminates de lithium et de sodium. II - spectres raman et infrarouge de $\text{Li}_3\text{AlH}_n\text{D}_{6-n}$ ($n = 0,1,2,4,5,6$). *Materials Research Bulletin*, 24(2), 133–141. [https://doi.org/10.1016/0025-5408\(89\)90117-7](https://doi.org/10.1016/0025-5408(89)90117-7)
- [23] Awbery, R. P., Broughton, D. A., & Tsang, S. C. (2008). In situ observation of lithium hydride hydrolysis by DRIFT spectroscopy. *Journal of Nuclear Materials*, 373(1-3), 94–102. <https://doi.org/10.1016/j.jnucmat.2007.05.039>

- [24] Montagnac, G. (2023, May 10). *Normalized Raman spectrum of TiO₂ anatase acquired with a 532 nm laser / REAP / SSHADE*. Wwww.sshade.eu.
https://www.sshade.eu/data/spectrum/SPECTRUM_GM_20190905_005
- [25] Montagnac, G. (2023, May 10). *Normalized Raman spectrum of TiO₂ rutile acquired with a 532 nm laser / REAP / SSHADE*. Wwww.sshade.eu.
https://www.sshade.eu/data/spectrum/SPECTRUM_GM_20190905_004
- [26] Luchinskii, G.P. (1966). Parameters of Phase Transitions of Titanium Tetrachloride. *Physico-Chemical Study of Titanium Halides.*, 40, 593-598.
- [27] Bridgeman, O.C.; Aldrich, E.W. (1964). Vapor Pressure Tables for Water, *J. Heat Transfer*, 86, 2, 279-286, <https://doi.org/10.1115/1.3687121>.

Appendix A – Spent Fuel Characterization

A.1 Optical Microscopy

As part of the project's qualitative analysis on spent fuel, an optical microscope is useful for generating particle size distribution graphs. Collecting size distribution graphs of the expected individual components of spent fuel to compare with a spent fuel sample may tell us if particle sizes change between before and post-reaction. This ex-situ characterization approach enables us to discern any potential influences on fuel reactivity.

Components of spent fuel were ground in a mortar and pestle and molecularly sieved. The 35–43-micron fraction was analyzed with an Olympus BX53 Microscope to obtain a particle size distribution. Microscope images were exported to ImageJ to measure particle diameters. To convert from pixels to microns, we measured known values at each magnification (4x, 10x, 40x) to convert the pixel measurement to micrometers. In ImageJ, particle diameters were measured manually, with the results being exported to Excel to plot particle size distribution for each component. This same process was repeated for the industry spent fuel (before and after grinding).

Safety precautions involve the mortar and pestle when powders are grinded. In addition to wearing eye protection glasses in the lab, nitrile gloves were worn to avoid contact with caustic properties as well as worn masks to reduce inhalation of particles that may irritate nasal passages.

Spent fuel particle distribution (comparing **Figure 9** and **Figure 11**) provides more information on the clumping size than the actual particle size; this information can be extracted from SEM images at much higher magnifications than the optical microscope (see **Appendix A.2**). Due to time, the group was unable to obtain particle sizing with SEM imaging. While under the microscope, it was observed that clumping of Alumina and Lithium Aluminate (**Figure 8**) was similar to spent fuel clumping (**Figure 10**).

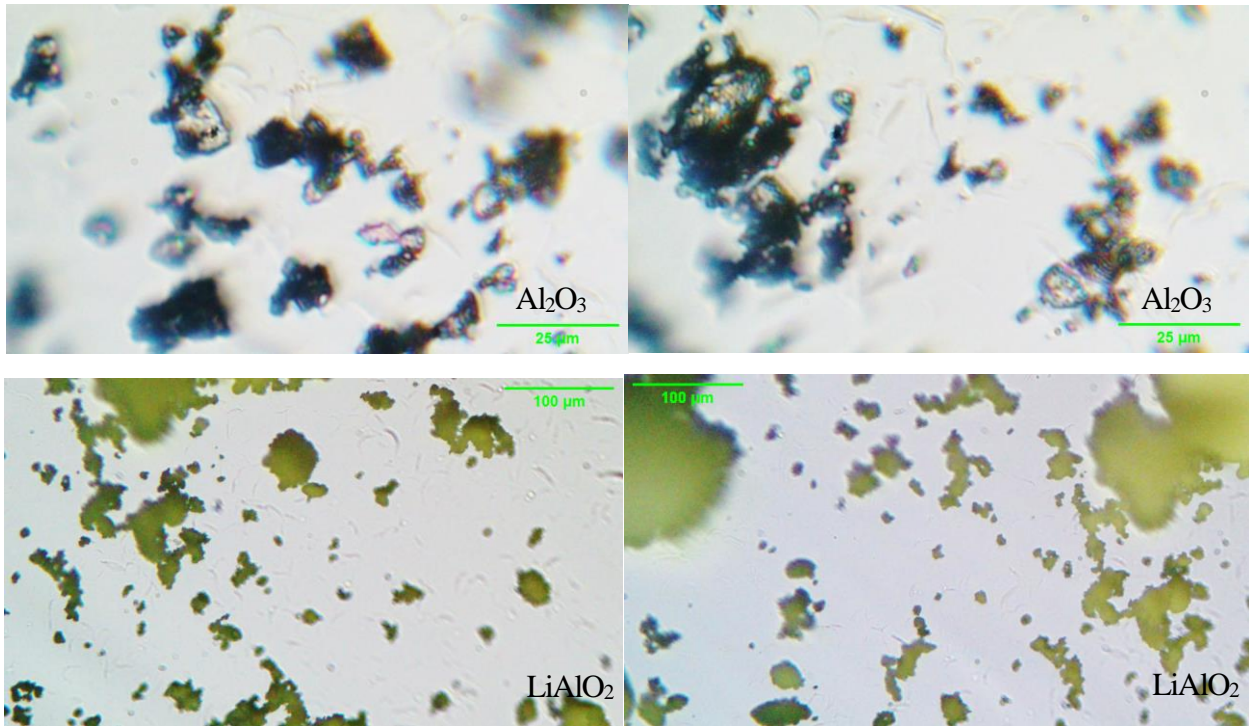


Figure 8. Images of spent fuel components (Al_2O_3 and LiAlO_2) under an Olympus BX53 Microscope.

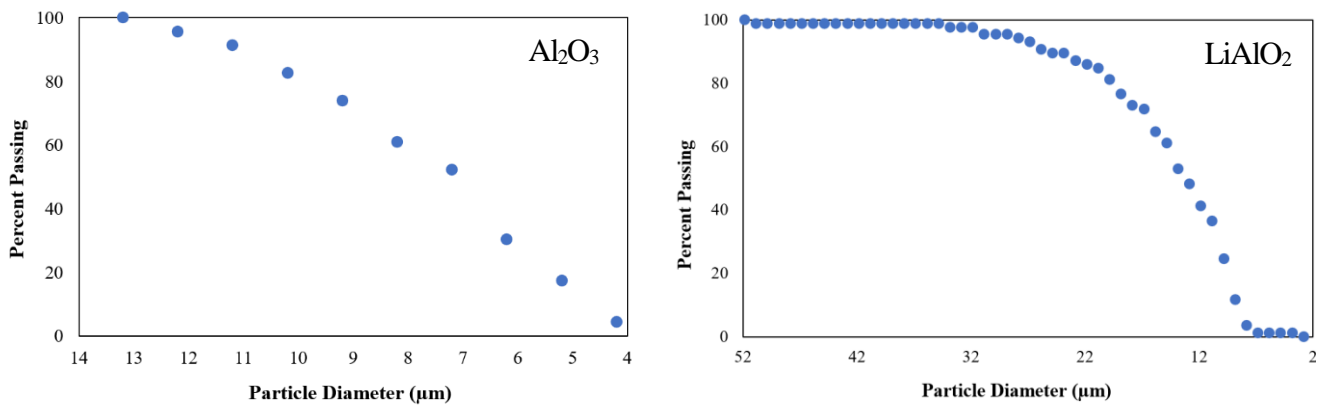


Figure 9. Particle distribution graphs of Al_2O_3 (left) and LiAlO_2 (right) based on manual measurements on ImageJ.

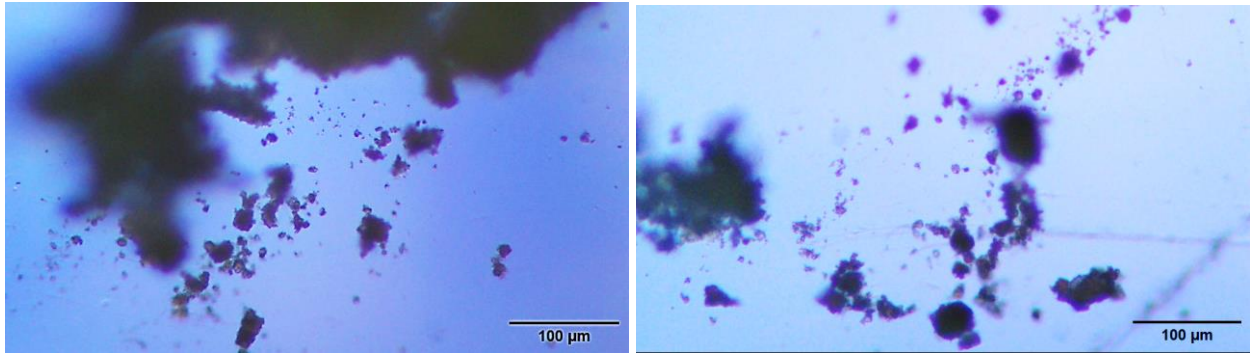


Figure 10. Images of spent fuel (light) under an Olympus BX53 Microscope.

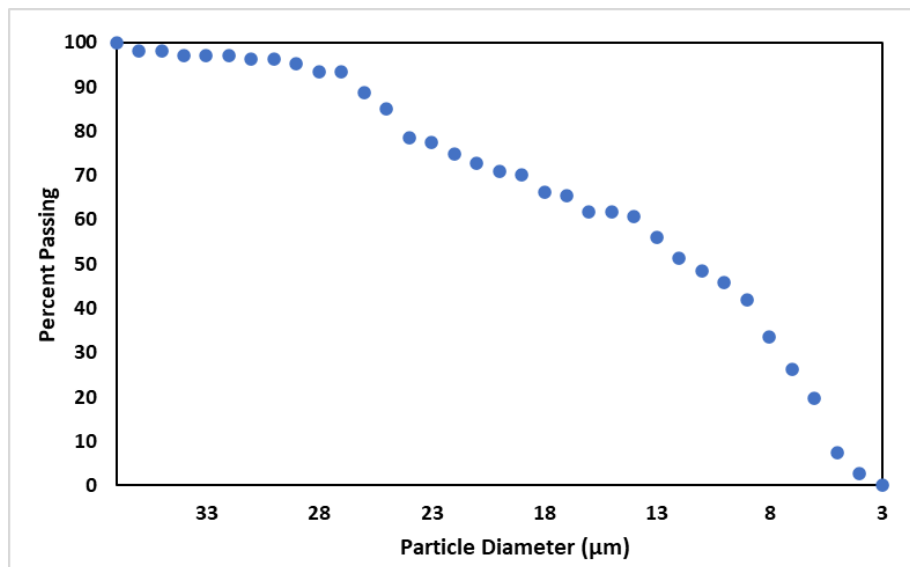


Figure 11. Particle distribution graph of Spent Fuel (Light) based on manual measurements on ImageJ.

A.2 SEM Scans

Figures 12 through 15 display SEM images of known spent fuel components at different magnifications. EDX was not performed alongside as chemical composition is already known— Al_2O_3 , $\text{Al}(\text{OH})_3$, LiAlO_2 , and LiOH bulk solid samples were purchased from Sigma Aldrich.

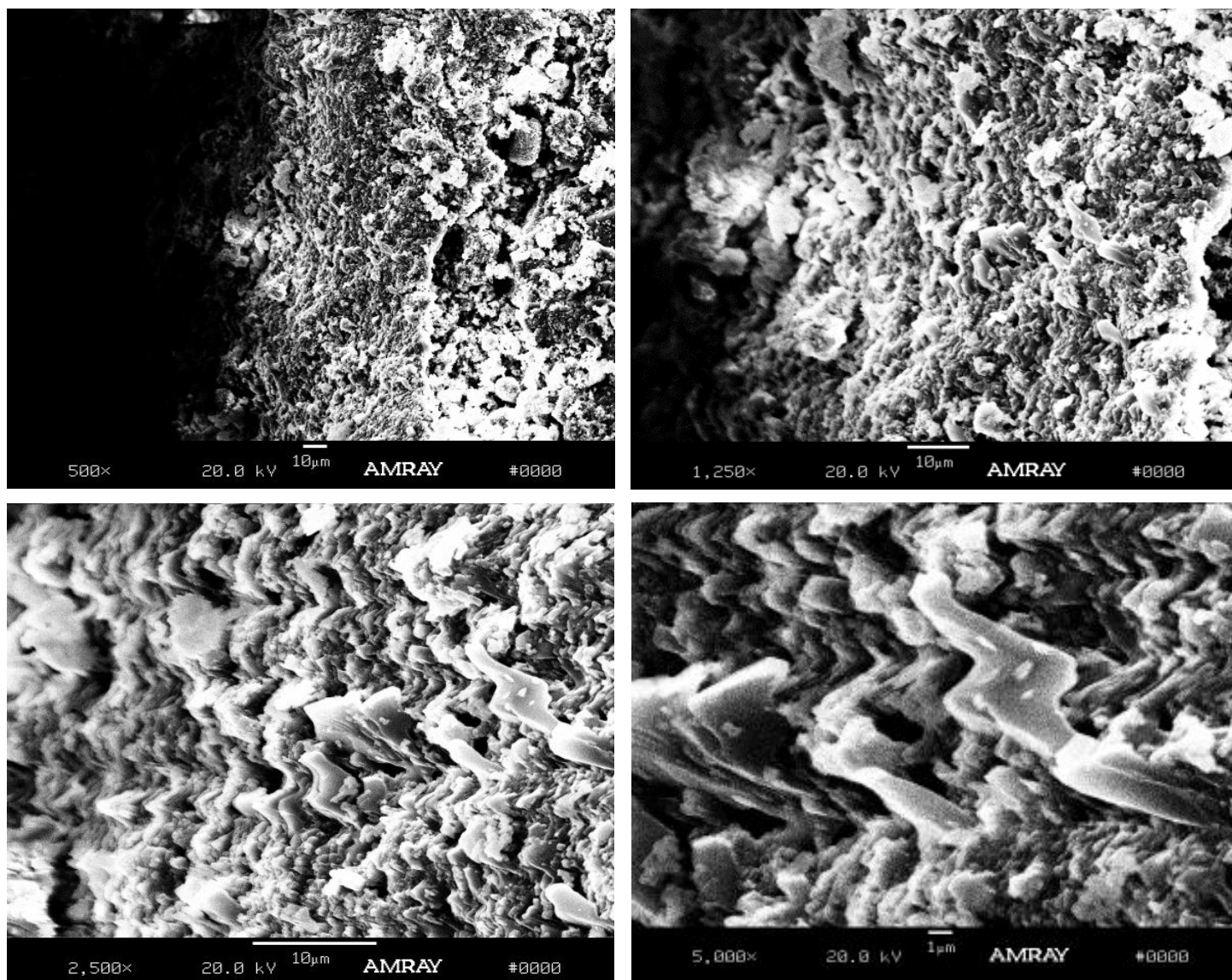


Figure 12. SEM Scans of Al_2O_3 (a known spent fuel component) at 500, 1250, 2500, and 5000x magnifications.

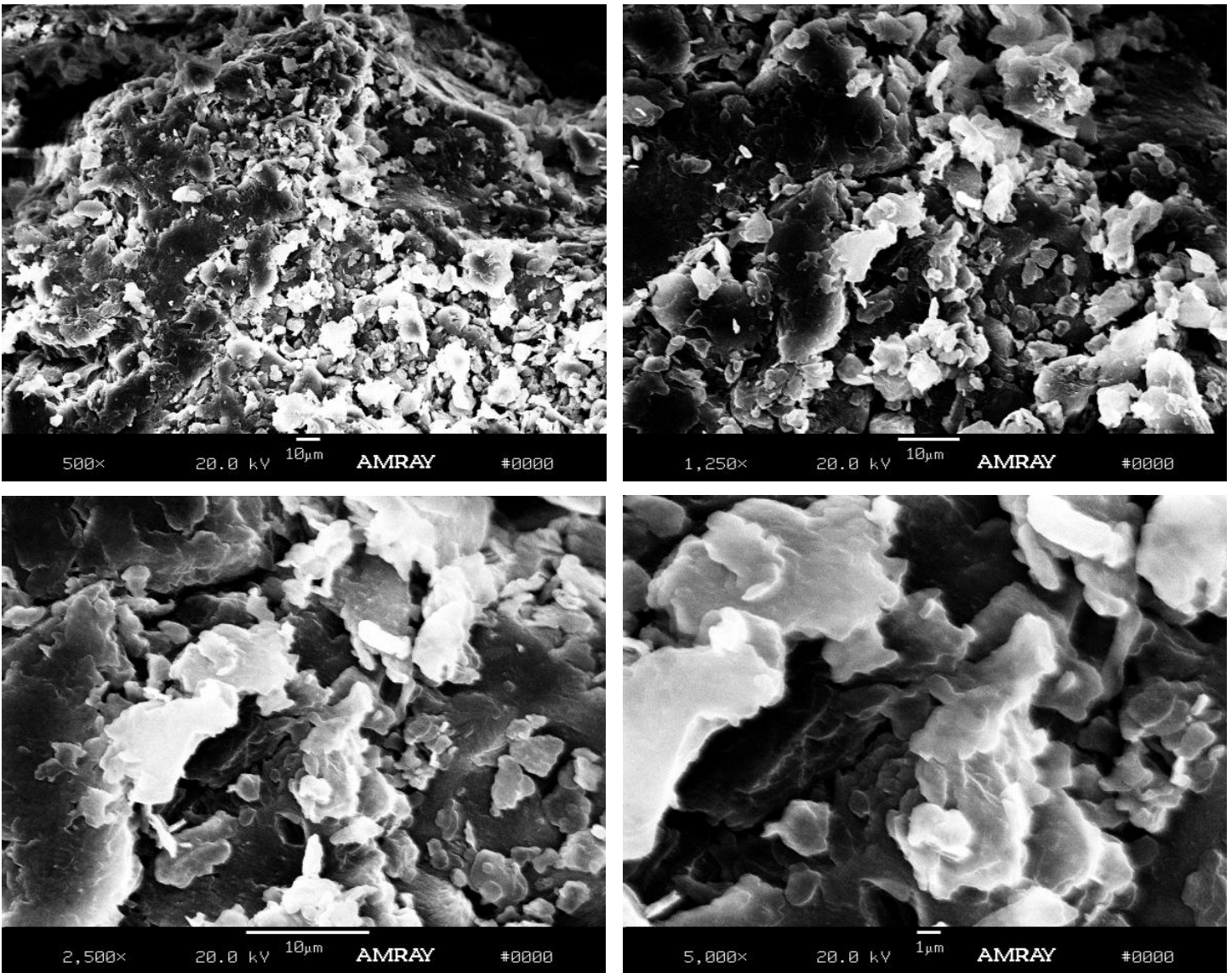


Figure 13. SEM Scans of $\text{Al}(\text{OH})_3$ (a known spent fuel component) at 500, 1250, 2500, and 5000x magnifications.

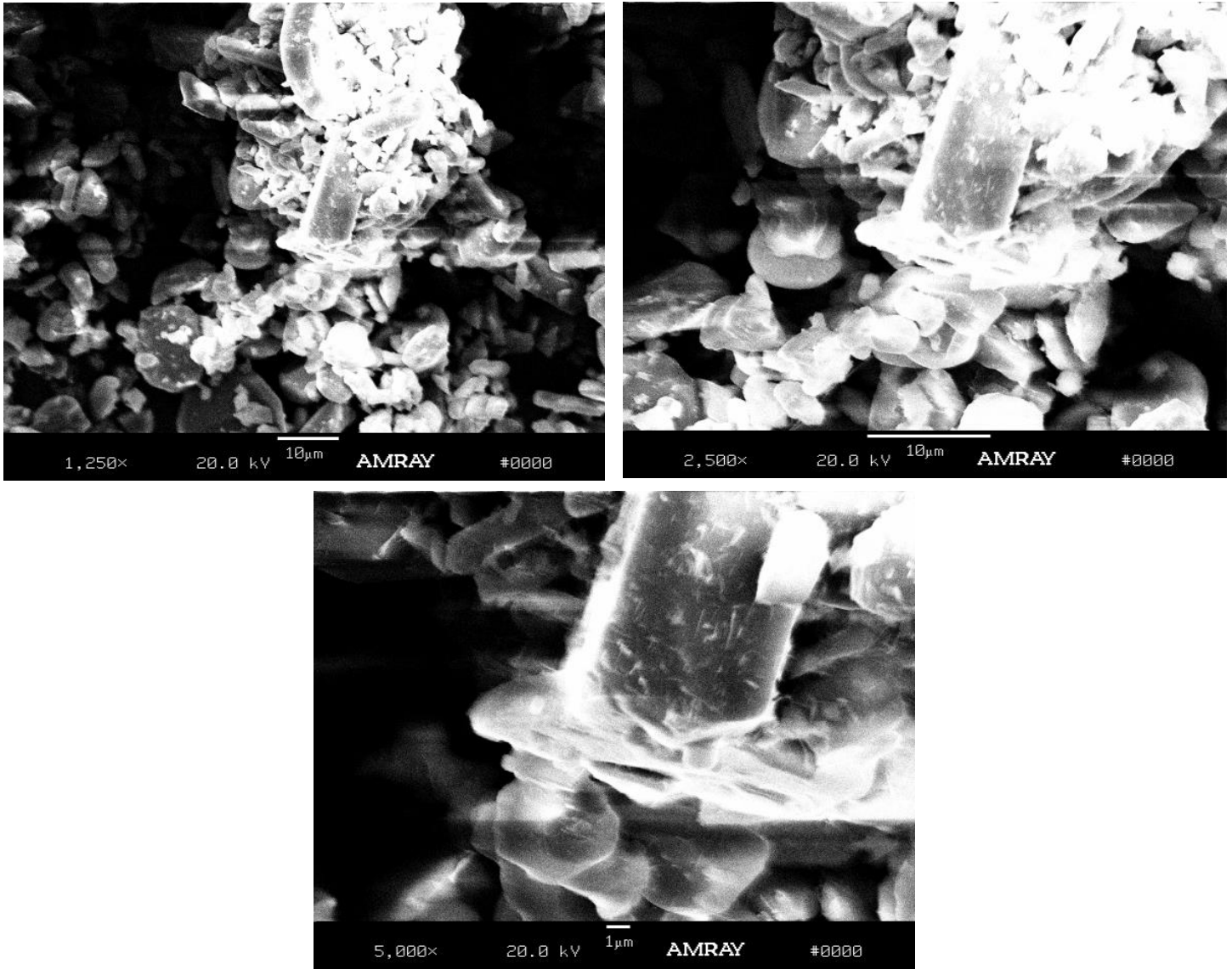


Figure 14. SEM Scans of LiAlO_2 (a known spent fuel component) at 1250, 2500, and 5000x magnifications.

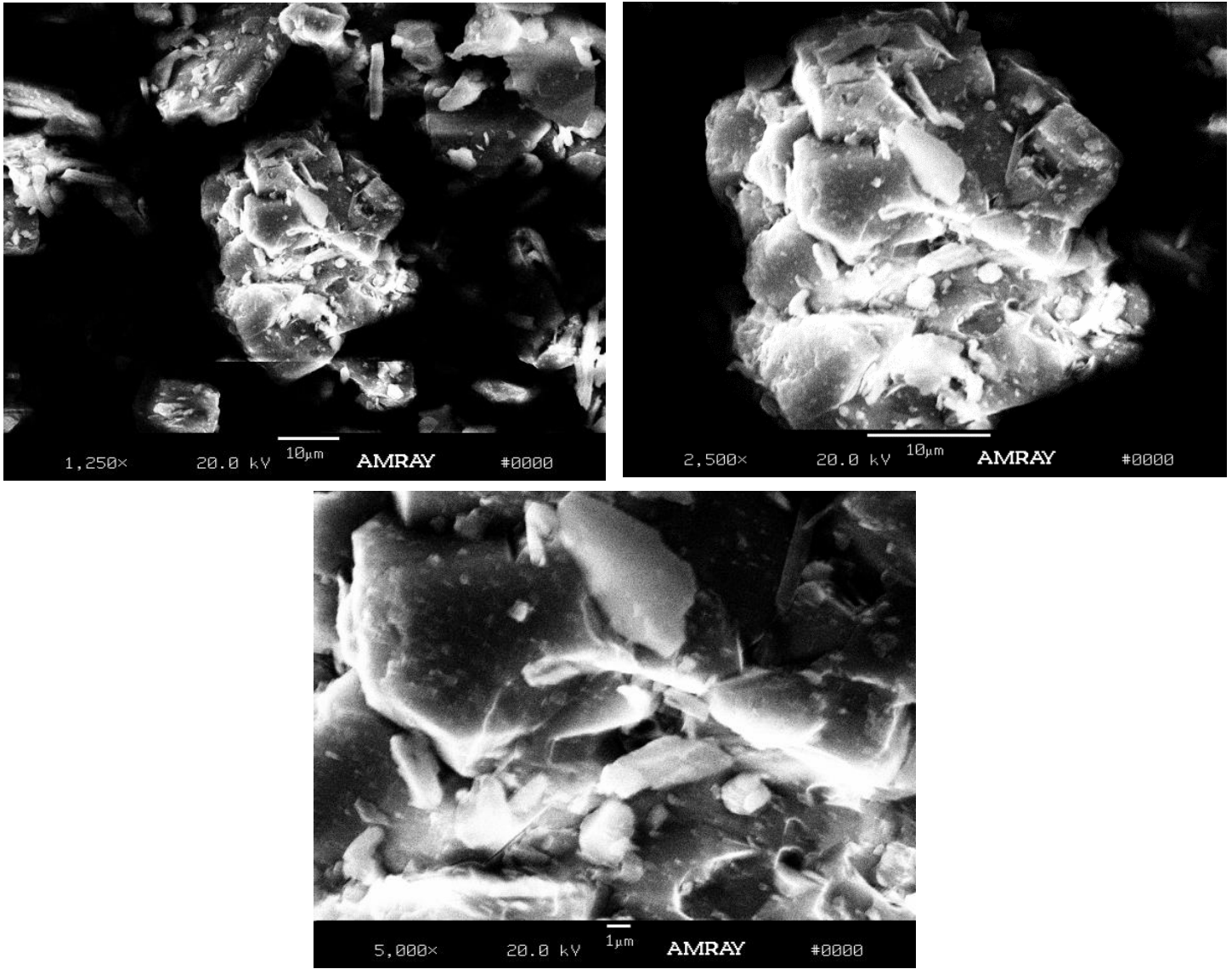


Figure 15. SEM Scans of LiOH (a known spent fuel component) at different magnifications.

A.3 SEM-EDX Spectra

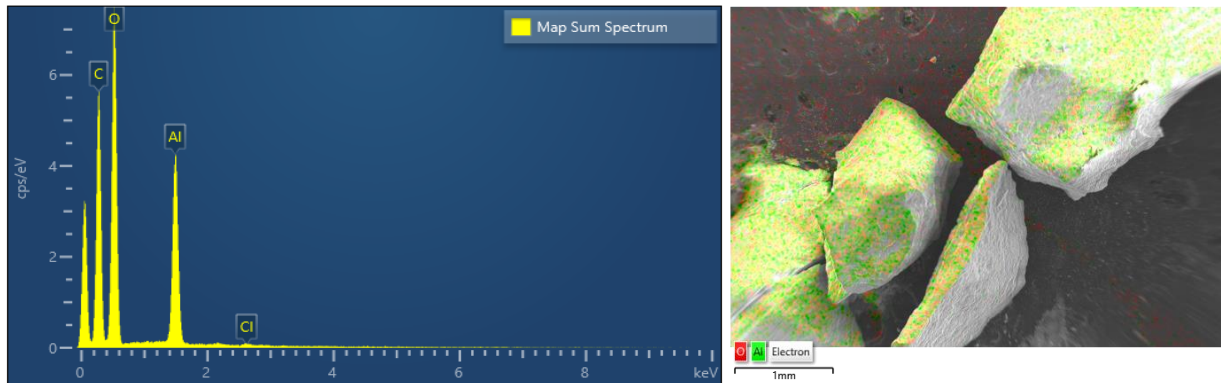


Figure 16. SEM/EDX spectrum and layered image of untreated spent fuel (Control)

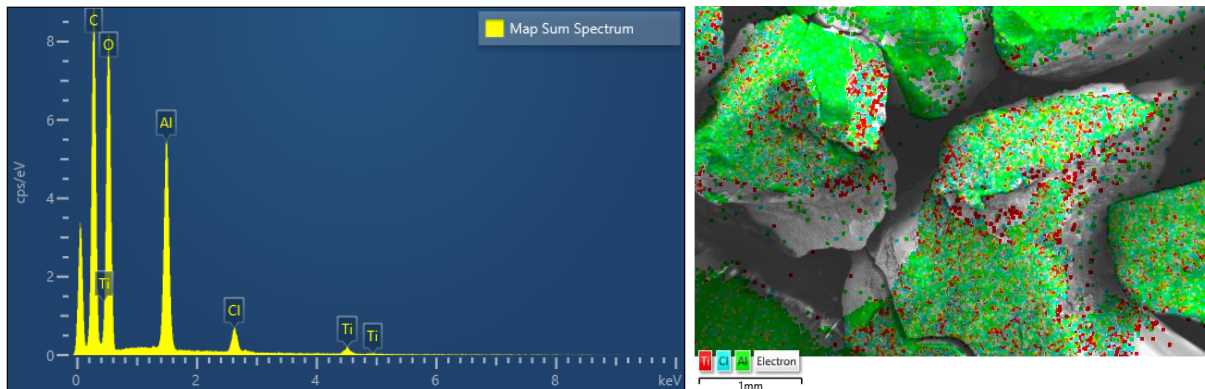


Figure 17. SEM/EDX spectrum and layered image of spent fuel treated in flow reactor

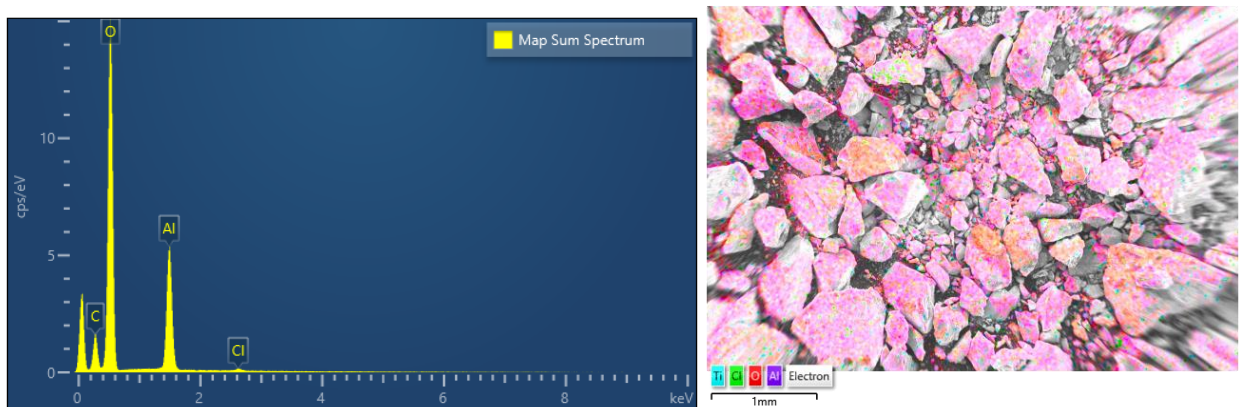


Figure 18. SEM/EDX spectrum and layered image of pre-hydrated spent fuel treated in batch reactor

A.4 XRD Spectra

X-Ray Diffraction analysis (XRD) is a technique used primarily in geology to study compositions of geodes or rocks. It is a non-destructive analysis method used to measure chemical composition, physical properties, and crystal structure of a sample. In the apparatus, a sample is radiated using X-rays which then get refracted by the crystalline structure. The diffracted X-rays are altered by the sample and the impression from the sample gets read by sensors in the apparatus. The intensity of the diffracted rays is plotted to represent a diffraction pattern. Each phase of the sample demonstrates a different diffraction depending on chemistry and specific arrangement.

The XRD was used to obtain insight on spent fuel composition. The known spent fuel components (LiOH , LiAlO_2 , Al_2O_3 , $\text{Al}(\text{OH})_3$) were ground (≈ 10 mg each) using a mortar and pestle in a glove bag. **Figure 19** shows similar peaks of spent fuel with LiAlO_2 (at 29 and 74 degrees) and $\text{Al}(\text{OH})_3$ (38 and 68 degrees). There may be similar peaks within the 30-40 degree range but peaks shifts have not been identified. Different industry spent fuel samples were looked at as well in **Figure 20** on the next page.

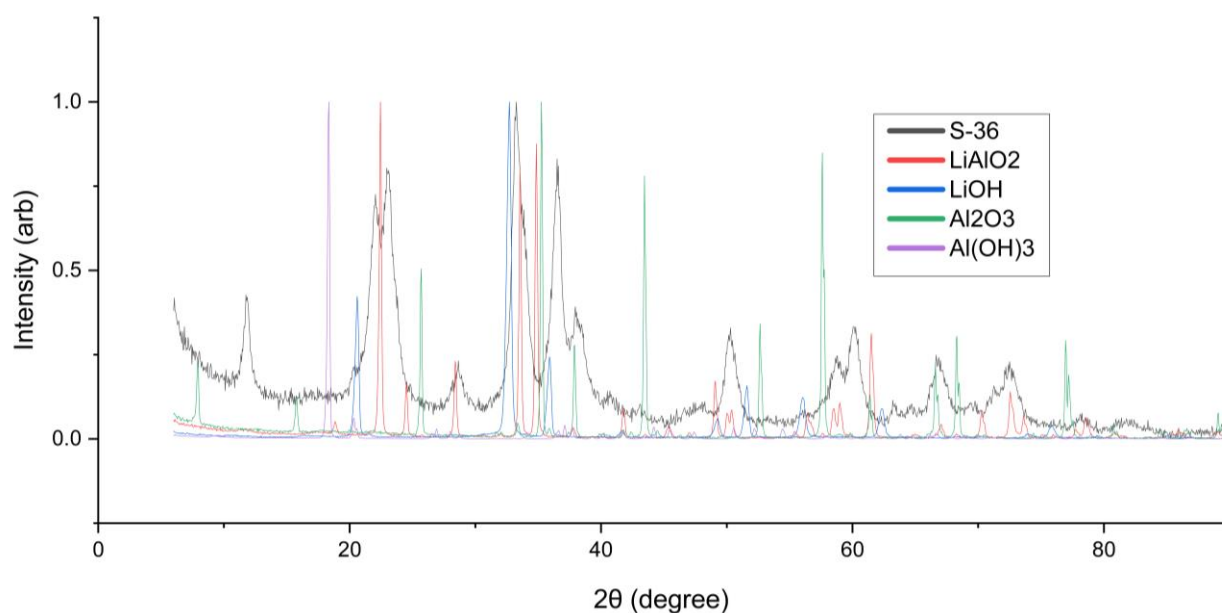


Figure 19. Normalized XRD Spectra of industry spent fuel (S-36, gray), LiAlO_2 (red), LiOH (blue), Al_2O_3 (green), and $\text{Al}(\text{OH})_3$ (purple).

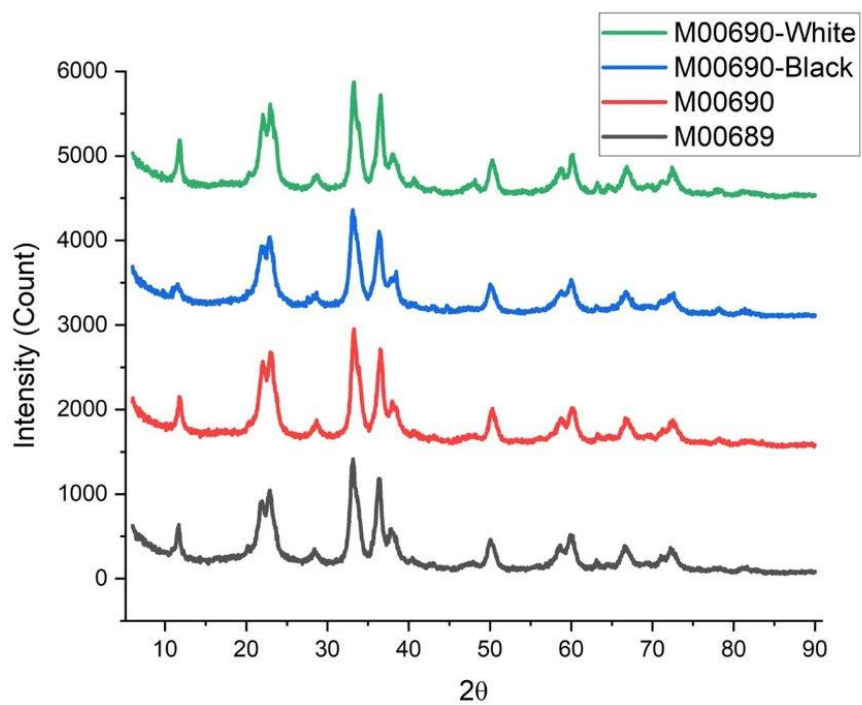


Figure 20. XRD Spectra of different types of industry spent fuel samples.

The XRD spectra comparison in **Figure 20** shows very minimal differences in chemical composition between the different types of industrial spent fuel samples.

$$\ln \left(\beta \int_0^\alpha \frac{d\alpha}{f(\alpha)} \right) = \ln \left\{ [A(\alpha)] \left[\int_{T_1}^{T_2} e^{\left(\frac{-E(\alpha)}{RT} \right)} dT \right] \right\} \quad \text{[Eqn. 2]}$$

$$\ln(\beta) = 5.3305 + \ln \left(\frac{A(\alpha)}{\int_0^\alpha \frac{d\alpha}{f(\alpha)}} \right) - \left[1.052 \frac{E(\alpha)}{R} \right] \left[\frac{1}{T} \right] \quad \text{[Eqn.3]}$$

Where:

$$y = \ln(\beta) \quad x = \frac{-1}{T}$$

$$m = 1.052 \frac{E(\alpha)}{R} \quad b = 5.3305 + \ln \left(\frac{A(\alpha)}{\int_0^\alpha \frac{d\alpha}{f(\alpha)}} \right)$$

Table 4. Thermal Gravimetric Analysis Conditions for Experimental Runs.

Material	Sample Mass (mg)	Set Temperature Range (°C)	Ramp Time (°C/min)
LiOH	10.4	100-600	5
	10.5	0.100-600	10
Al(OH)₃	10.2	25-600	5
	10.5	25-600	15
LAH	9.5	25-600	5
	8.9	25-600	10
	8.2	25-600	20

LiAlO₂, Al₂O₃, spent fuel did not run due to time constraints. TGA graphs are presented on pages

Adsorption Thermodynamics

LAH, spent fuel, and known spent fuel components can be ran in the TGA instrument to study adsorption thermodynamics as well. At least three different isotherms for a measured amount of time is necessary to graph the relationship.

Water's heat of adsorption on LAH is pertinent information as it affects how safe the material can be transported. Higher water adsorption properties for LAH increases the chance of unspent fuel still lingering to potentially react with water molecules trapped on the surface and risk an unintended explosion. To understand the extent of this danger, TGA can also obtain thermodynamic information. In this case, different isotherms of a material can be plotted to extract the activation energy of water's heat of adsorption onto LAH

surface. The Clausius – Clapeyron Equation describes the relationship between a material's temperature and vapor pressure as shown in **Equation 3** below. The slope of the plotted graph

$$\frac{dp}{dT} = \frac{\Delta H}{T\Delta V} \quad [\text{Eqn. 3}]$$

$$\ln(p) = -\frac{\Delta H}{RT} + C$$

$$\ln \frac{p_2}{p_1} = \frac{\Delta H}{R} \left(\frac{1}{T_1} - \frac{1}{T_2} \right)$$

$$\ln(p) = k \frac{\Delta H}{R} \times \frac{1}{T} \quad [\text{Eqn. 4}]$$

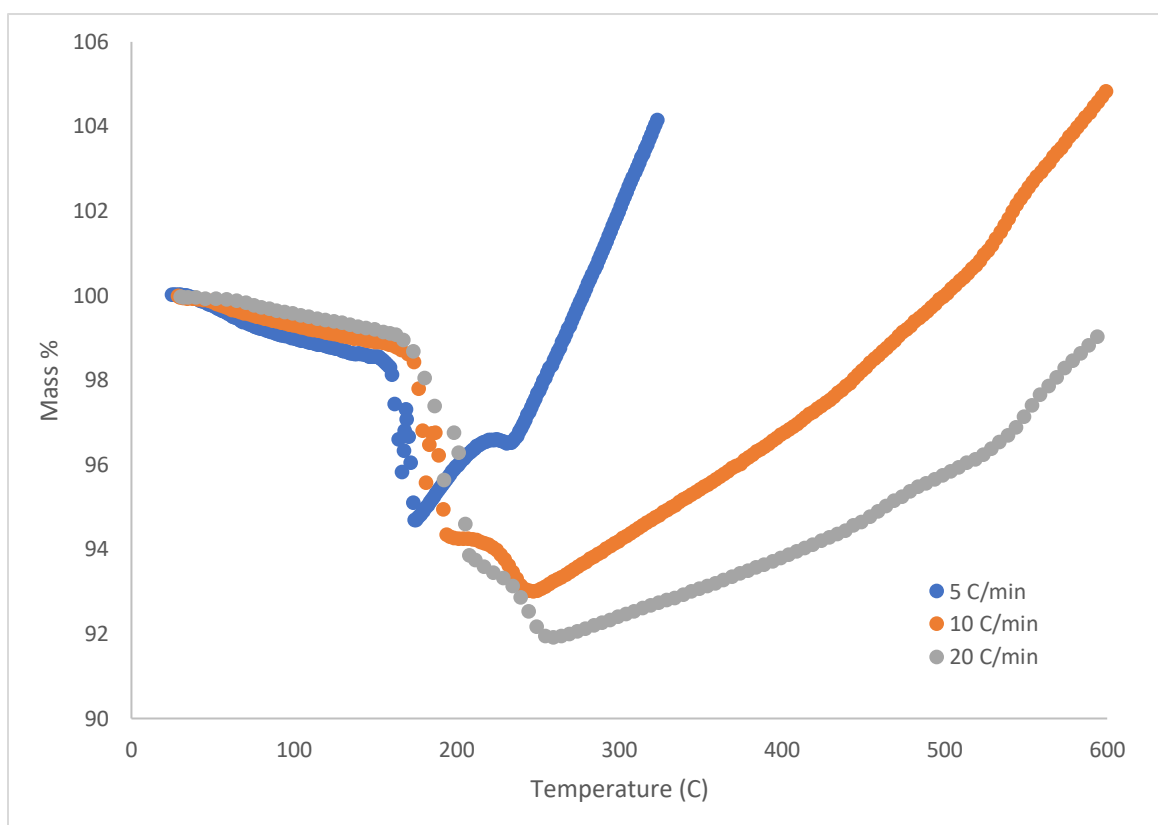


Figure 21. Mass loss of LAIH₄ in a N₂ atmosphere at 5, 10, and 20 °C/min heating rates. The initial drop in mass may be water loss. The following step drop roughly aligns with thermolysis. Towards the end of thermolysis, the sample begins to gain mass once again, presumably from a reaction with the nitrogen atmosphere. A higher heating rate appears to have resulted in a greater extent of reaction.

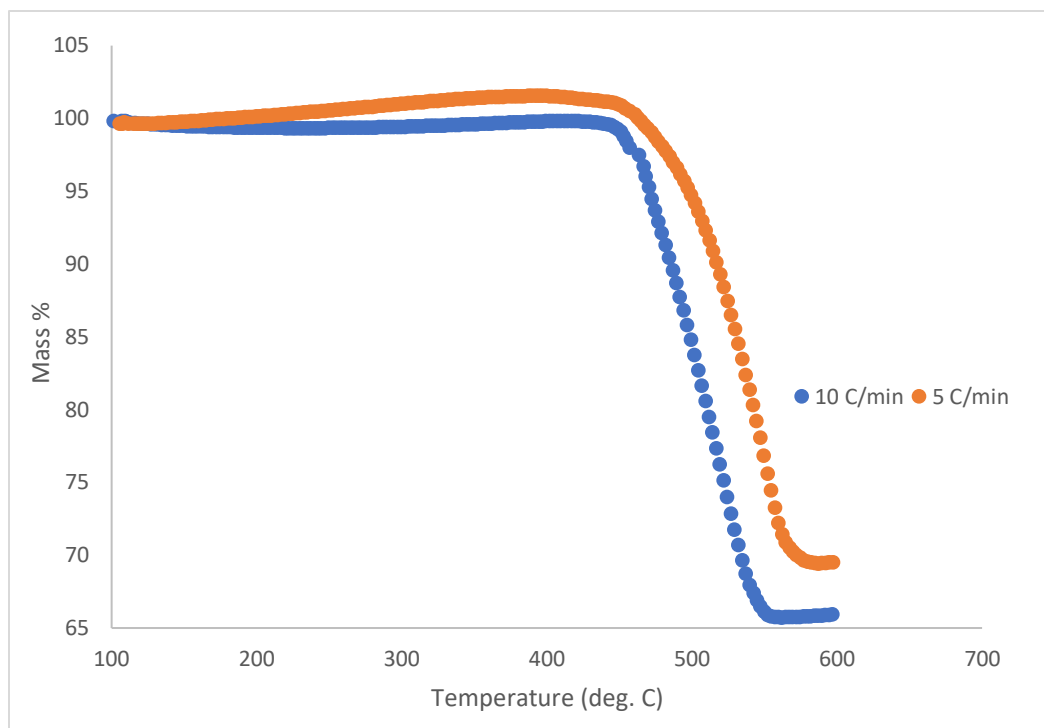


Figure 22. Mass loss of LiOH in a N₂ atmosphere at 5 and 10 °C/min heating rate.

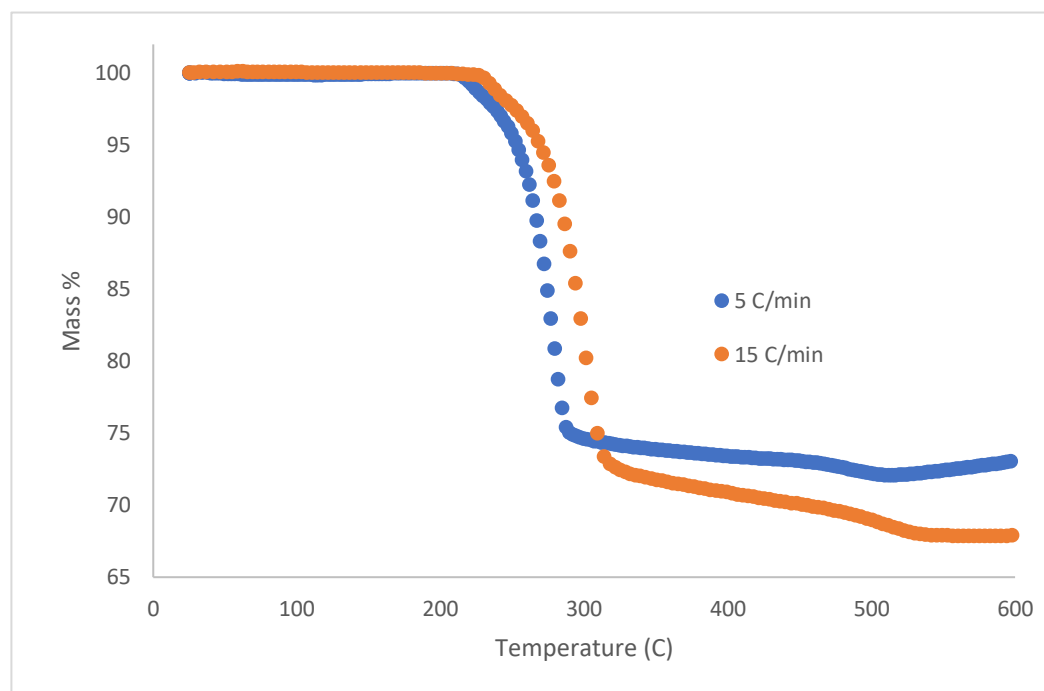


Figure 23. Mass loss of Al(OH)₃ in a N₂ atmosphere at 5 and 15 °C/min heating rate.

Appendix B – Preliminary Batch Experimentation

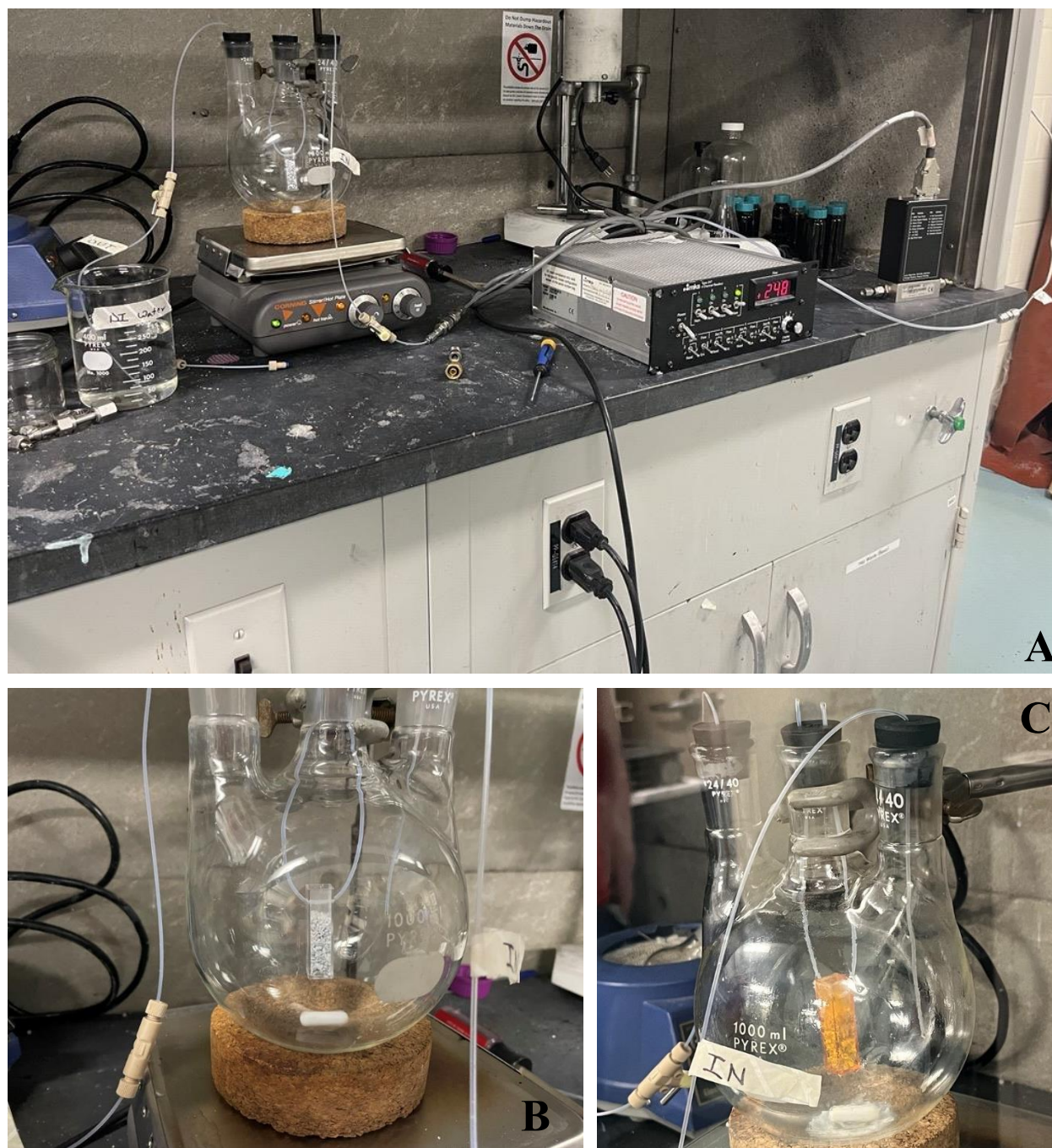


Figure 24. First apparatus setup of batch synthesis experiment

The initial runs of the batch reaction experienced several difficulties. Firstly, the plastic cuvette used to hold the sample reacted, turning orange and pliable. The rubber stoppers used were arranged in such a way that there could be no easy injection into the apparatus. The tubing was later rearranged, and a septum was used. The surface area of the sample which could be accessed by the TiCl_4 vapors were severely limited by the geometry and mixing of the vessel. Vapor would first have to reach above the sample container, then travel through the sample, making exposure to vapor primarily on the surface layer of the sample.

A problem which persisted in all batch reactions was difficulty in removing the sample from the vessel without spilling any. Because the sample was suspended using plastic tubing, the tubing would get stuck in the neck of the vessel, tipping the container. Additional improvements to be made to the batch setup include In terms of safety, better pressure controls would be appropriate to monitor the buildup of pressure due to clogging from solids. The water trap used should also be improved with greater dispersion of the gas bubbles and longer exposure to the water. The setup used resulted in some partially reacted TiCl_4 vapor exiting the system, as well as HCl gas.

Appendix C - Flow Experiment Calculations

C.1 Saturated Vapor Density Calculations

The vapor pressure of a pure liquid in equilibrium can be found from the Antoine equation. The number of moles of this vapor in a gas mixture can then be found.

Antoine Equation:

$$\log_{10} p^* = A - \left(\frac{B}{T + C} \right)$$

Ideal Gas Law:

$$PV = nRT$$

For an Ideal Gas Mixture:

$$\frac{p_i}{P} = \frac{n_i}{n}$$

Moles of Saturated Vapor in an Ideal Gas Mixture:

$$n_i = \frac{p^*V}{RT}$$

Where:

A, B, C = Antoine equation constants

p^* = vapor pressure (bar)

T = Temperature (K)

n = total number of moles

P = total pressure (bar)

V = volume (m³)

R = 8.3145*10⁻⁵ m³ bar K⁻¹mol⁻¹

p_i = partial pressure of gas i (bar)

n_i = number of moles of component i

Table 5. Antoine equation constants and calculated values at 298 K^{26,27}

Chemical	A	B	C	Value at 298 K (Bar)
TiCl ₄	4.84969	1990.235	2.0	0.016428
H ₂ O	5.40221	1838.675	-31.737	0.03136

Table 6. Saturated Vapor Density at 298 K

Chemical	Sat. vapor molar density (mol/ml)	Sat. vapor density (mg/ml)
TiCl ₄	6.630*10 ⁻⁷	0.1258
H ₂ O	1.266*10 ⁻⁶	0.0228

Sample Calculation:

For the TiCl₄ bubbler:

$$P = 1 \text{ bar}$$

$$T = 298 \text{ K}$$

$$V = 0.000001 \text{ m}^3$$

Let gas 1 be TiCl₄ and gas 2 makeup argon:

$$p^* = 10^{4.84969 - \left(\frac{1990.235}{298+2}\right)} = 0.016428$$

$$n_i = \frac{0.016428 * 0.000001}{8.3145 * 10^{-5} * 298} = 6.630 * 10^{-6}$$

C.2 Theoretical Yield Calculations

Assuming all gas is exiting the bubblers saturated in TiCl_4 or H_2O allows for estimation of the mass of TiO_2 generated. Assuming the reaction immediately goes to completion and with 100% yield:

In the case TiCl_4 is limiting:

$$m_{\text{TiO}_2} = Q\rho_{\text{TiCl}_4}t$$

In the case water is limiting:

$$m_{\text{TiO}_2} = Q\rho_{\text{H}_2\text{O}}t$$

Where:

m_{TiO_2} = mass of TiO_2 created by the reaction (mg)

Q = total gas flowrate (ml/s)

ρ_i = saturated vapor density (mg/ml)

t = time (s)

Table 7. Experimental parameters of flow synthesis experiment.

Water Exposure Time (s)	Wet line flow rate (ml/s)	TiCl_4 Exposure Time (s)	TiCl_4 line flow rate (ml/s)	Theoretical Mass of TiO_2 (mg)	Sample Initial Mass (mg)	Sample final Mass (mg)	Measured Mass Difference (mg)
1200	1.38	300	1.30	49.1	445.2	474.6	29.4

C.3 Water Sorption Testing

Table 8. Experimental runs of water sorption.

Time (s)	Gas Flow Rate (ml/s)	Sample Starting Mass (g)	Sample End Mass (g)	Sample wt% water
1200	1.38	0.5034	0.524	3.93
1200	1.38	0.4459	0.4569	2.41
1200	1.38	0.4731	0.4779	1.00
3600	1.38	0.4732	0.5118	7.54

C.4 Mass Flow Controller Calibration Curves

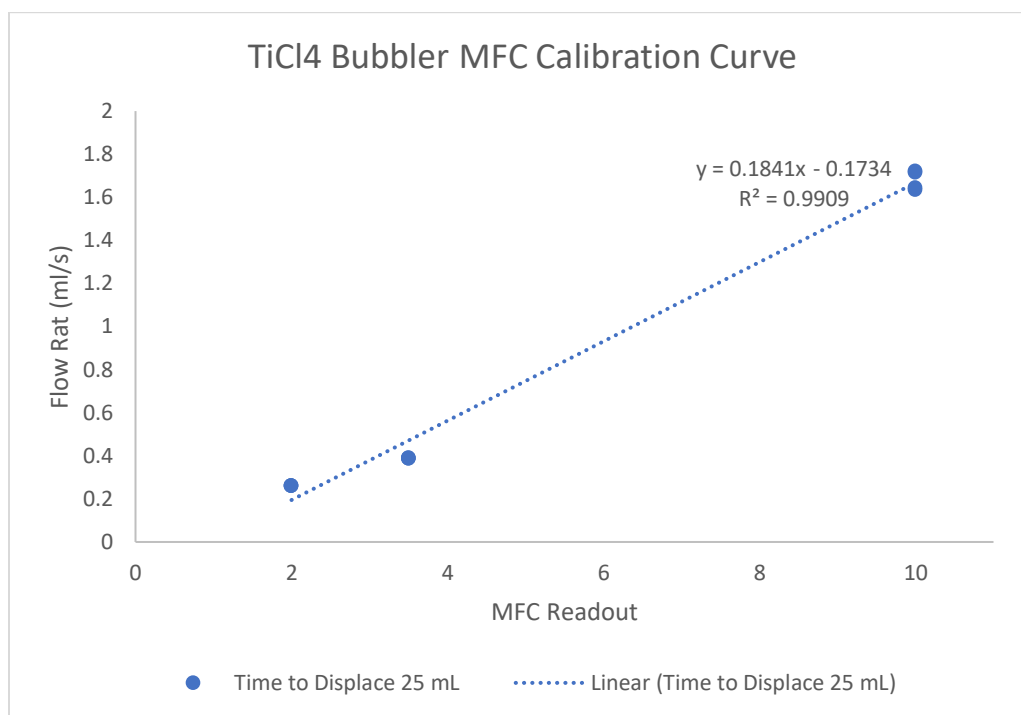


Figure 25. TiCl_4 bubbler mass flow controller calibration curve obtained using a bubble meter.

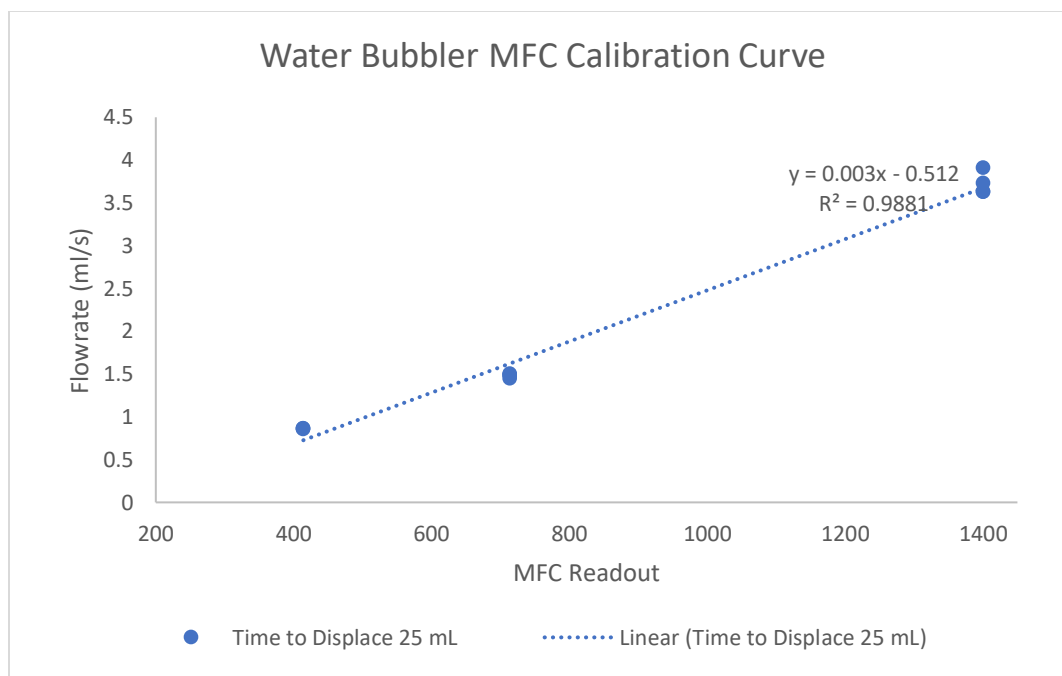


Figure 26. Water bubbler mass flow controller calibration curve obtained using a bubble meter.